



OPEN ACCESS

EDITED BY

Ángel Puga-Bernabéu,
University of Granada, Spain

REVIEWED BY

Ahmed Radwan,
Jagiellonian University, Poland
Pura Alfonso,
Universitat Politècnica de Catalunya,
Spain

*CORRESPONDENCE

Khalid Al-Ramadan,
✉ ramadank@kfupm.edu.sa
Abdulwahab Muhammad Bello,
✉ abdulwahab.bello@kupm.edu.sa

RECEIVED 22 November 2022

ACCEPTED 04 April 2023

PUBLISHED 14 April 2023

CITATION

Bello AM, Al-Ramadan K,
Koeshidayatullah AI, Amao AO,
Herlambang A, Al-Ghamdi F and
Malik MH (2023), Impact of magmatic
intrusion on diagenesis of shallow marine
sandstones: An example from Qasim
Formation, Northwest Saudi Arabia.
Front. Earth Sci. 11:1105547.
doi: 10.3389/feart.2023.1105547

COPYRIGHT

© 2023 Bello, Al-Ramadan,
Koeshidayatullah, Amao, Herlambang, Al-
Ghamdi and Malik. This is an open-access
article distributed under the terms of the
[Creative Commons Attribution License
\(CC BY\)](https://creativecommons.org/licenses/by/4.0/). The use, distribution or
reproduction in other forums is
permitted, provided the original author(s)
and the copyright owner(s) are credited
and that the original publication in this
journal is cited, in accordance with
accepted academic practice. No use,
distribution or reproduction is permitted
which does not comply with these terms.

Impact of magmatic intrusion on diagenesis of shallow marine sandstones: An example from Qasim Formation, Northwest Saudi Arabia

Abdulwahab Muhammad Bello^{1*}, Khalid Al-Ramadan^{1,2*},
Ardiansyah I. Koeshidayatullah², Abduljamiu O. Amao¹,
Adhipa Herlambang¹, Faisal Al-Ghamdi¹ and Muhammad H. Malik²

¹Center for Integrative Petroleum Research, College of Petroleum Engineering and Geosciences, King Fahd University of Petroleum and Minerals, Dhahran, Saudi Arabia, ²Geosciences Department, College of Petroleum Engineering and Geosciences, King Fahd University of Petroleum and Minerals, Dhahran, Saudi Arabia

Igneous intrusions are common in sedimentary basins, and their occurrence can significantly affect the diagenesis and reservoir quality evolution of sandstones, thereby strongly impacting their hydrocarbons-, geothermal-, and CO₂-storage potentials. The Qasim sandstones in the Tabuk region (NW Saudi Arabia) experienced shallow burial diagenesis (<2 km) when the Tertiary magma intruded to form basaltic sills (0.4–4 m thick). The sedimentology, tectono-stratigraphic framework, provenance, and chemostratigraphy of the Qasim Formation have been extensively covered in the literature. However, the impact of the magmatic intrusion on diagenesis and reservoir quality evolution of the sandstones remains enigmatic. This study employed thin-section petrography, QEMSCAN, XRD, SEM, and energy-dispersive spectrometer analyses to investigate the role of magmatic intrusion on diagenesis and reservoir quality of the Qasim sandstones. The results of the study indicate that reservoir porosity is principally influenced by primary depositional characteristics (grain size and sorting), diagenetic alterations, and magmatic intrusions. Sandstones with coarser grain size and better sorting have the best intergranular porosity and *vice versa*. The “normal” diagenetic processes that have significantly affected the reservoir porosity of the sandstones occurred during both shallow burial (eodiagenesis) and uplift (telodiagenesis). The eogenetic alterations include mechanical compaction, early diagenetic cementation by calcite, pyrite, and kaolinite, whereas the telogenetic alterations include the formation of kaolinite, goethite, hematite. Overall, mechanical compaction is the main driver for porosity loss in the sandstones. The intrusion-related diagenetic processes include the dissolution of quartz grains, rounded quartz overgrowths, and calcite cement, and the transformation of kaolinite into dickite and chlorite. Detrital quartz and rounded quartz overgrowths have undergone dissolution due to acidic pore fluids from magma and high temperature. The transformation of kaolinite into dickite occurred in a dissolution-recrystallization fashion, and the amounts of kaolinite and dickite increase in fine-grained sediments away from sill contact due to hydrodynamic processes that deposited muscovite (which form kaolinite) in low energy environments. The chloritization of kaolinite was localized, and the

magma-induced dissolution of goethite likely supplied the requisite high Fe content. Additionally, the intrusion has resulted in the dissolution of the early calcite and increase in porosity towards the sill contact. However, values for compactional porosity loss have relatively remained similar both at and away from the sill contact, as the sill is too thin to exert significant vertical loading. This study has relevance to understanding hydrocarbon exploration and exploitation in sediment-lava sequences, and to understanding the development of sediment-lava systems.

KEYWORDS

Qasim Formation, magmatic intrusion, diagenesis, porosity, reservoir quality

1 Introduction

The quality of hydrocarbon reservoirs is strongly influenced by their burial history and the types of diagenetic alterations they have been subjected to (Koeshidayatullah and Al-Ramadan, 2014; Worden et al., 2018; Al-Ramadan et al., 2019; Hussain et al., 2022; Bello et al., 2023a; Bello et al., 2023b). Reservoir quality evolution pathways of sandstones are strongly controlled by several parameters, including detrital mineralogy, primary depositional facies, diagenesis, and composition and flow patterns of basinal fluids (Al-Ramadan et al., 2004; Al-Ramadan et al., 2017; Al-Ramadan, 2021; Bello et al., 2022a; Hussain et al., 2023). Therefore, understanding the processes that affect the reservoir quality of sandstones is of broad scientific and economic significance (Aro et al., 2023). Diagenetic processes involve the physical, chemical, and biological alterations that begin during or shortly after sediment deposition, which significantly affect the detrital composition of sediments, their texture, and fluid flow patterns in sandstone reservoirs (Morad et al., 2010; Al-Ramadan et al., 2017). For instance, diagenetic alterations are responsible for the formation of secondary porosity in sandstones through dissolution of unstable minerals, and are responsible for the preservation or destruction of primary porosity through the formation of grain-coating clays or precipitation of pore-filling cements, respectively (Bjørlykke, 1988; Ehrenberg, 1993; Bloch et al., 2002; Oluwadebi et al., 2018; Bello et al., 2022a; Bello et al., 2022b; Bello et al., 2022c). In addition, understanding the controls on sandstones diagenesis would significantly improve our ability to predict reservoir quality at local or basin scales (Worden et al., 2018).

Sandstone reservoirs are key exploration targets for hydrocarbons, geothermal energy, and CO₂ capture and storage (Al-Ramadan et al., 2005; Saner et al., 2006; Xia and Wilkinson, 2017; Hussain et al., 2018; Allen et al., 2020; Herlambang et al., 2022). Additionally, as the energy demand in the world is increasing, and hydrocarbon exploration moves towards deeper, more-challenging systems such as basins affected by igneous intrusion activity (Haile et al., 2019; Duffy et al., 2021; Rong et al., 2021), it is important to understand the interaction of diagenesis and magmatic intrusions on the reservoir quality of sandstones. This is primarily because magmatic intrusions can significantly impact diagenesis, thermal history, hydrocarbon source rock maturation, reservoir compartmentalization, and fluid migration pathways (Holford et al., 2012; Holford et al., 2013; Eide et al., 2017; Senger et al., 2017; Zahedi and MacDonald, 2018; Rong et al., 2021). Although sedimentary basins affected by magmatic intrusions are very

common (e.g., the Shetland Faroe Basin, North Atlantic margin) (Muirhead et al., 2017; Schofield et al., 2017), Songliao Basin, China (Rong et al., 2021), Nequen Basin, Argentina (Monreal et al., 2009), Carnarvon Basin, Australia (Holford et al., 2013), there is a growing need to understand the influence of intrusion-induced diagenesis in order to reduce the risk of exploration.

The Middle to Upper Ordovician Qasim Formation in the Tabuk region, northwest Saudi Arabia (Figure 1), is among the important Paleozoic reservoir rocks in central Saudi Arabia (Laboun, 2010). Additionally, the Qasim Formation (Quwarah Member) experienced shallow burial diagenesis (<2 km) (Laboun, 2010), when Tertiary magma, due to the opening of the Red Sea, intruded to form basaltic sills between 7.8 and 26.7 Ma (Grainger and Hanif, 1989). Although the volcanic events were short-lived and occurred at different time intervals, the impact of the intrusions on diagenetic alterations of the Qasim Formation is almost completely unknown. Furthermore, this geological formation is an ideal candidate for investigating the role of heat-flux related to short-lived, intrusion-induced diagenesis in the sandstones. The Qasim Formation is characterized by highly porous sandstones that have been intruded by well-exposed basaltic igneous rock during the Tertiary (Grainger and Hanif, 1989). Moreover, because the Qasim sandstones in the Tabuk region have never been deeply buried (Laboun, 2010), the effects of magmatic-induced diagenesis can be easily distinguished from “normal”, low-temperature diagenesis. Therefore, this paper aims to use a multi-technique approach involving thin section petrography, scanning electron microscopy (SEM), energy dispersive X-ray spectrometer (EDS), X-ray diffraction (XRD), and QEMSCAN[®] to investigate the effects of sill-induced diagenesis on reservoir quality evolution of the Qasim Formation.

2 Geological background

The study area is located at 27°45′49.8″N latitude and 36°35′06.9″E longitude, about 50 km south of the city of Tabuk, Saudi Arabia (Figures 1A, B). The area falls within the Shaghab quadrangle (Map GM-109C; Sheet 27B) described by Grainger and Hanif (1989). This area includes outcrops of the Middle to Upper Ordovician Qasim Formation (Senalp and Al-Duaiji, 2001; Laboun, 2010), which has been interpreted as the lower part of the Tabuk Formation (Senalp and Al-Duaiji, 2001). The Tabuk Formation was originally defined by Steineke et al. (1958), amended by Powers et al. (1966), and subsequently discarded following the recognition of regional unconformities within the formation. The Qasim

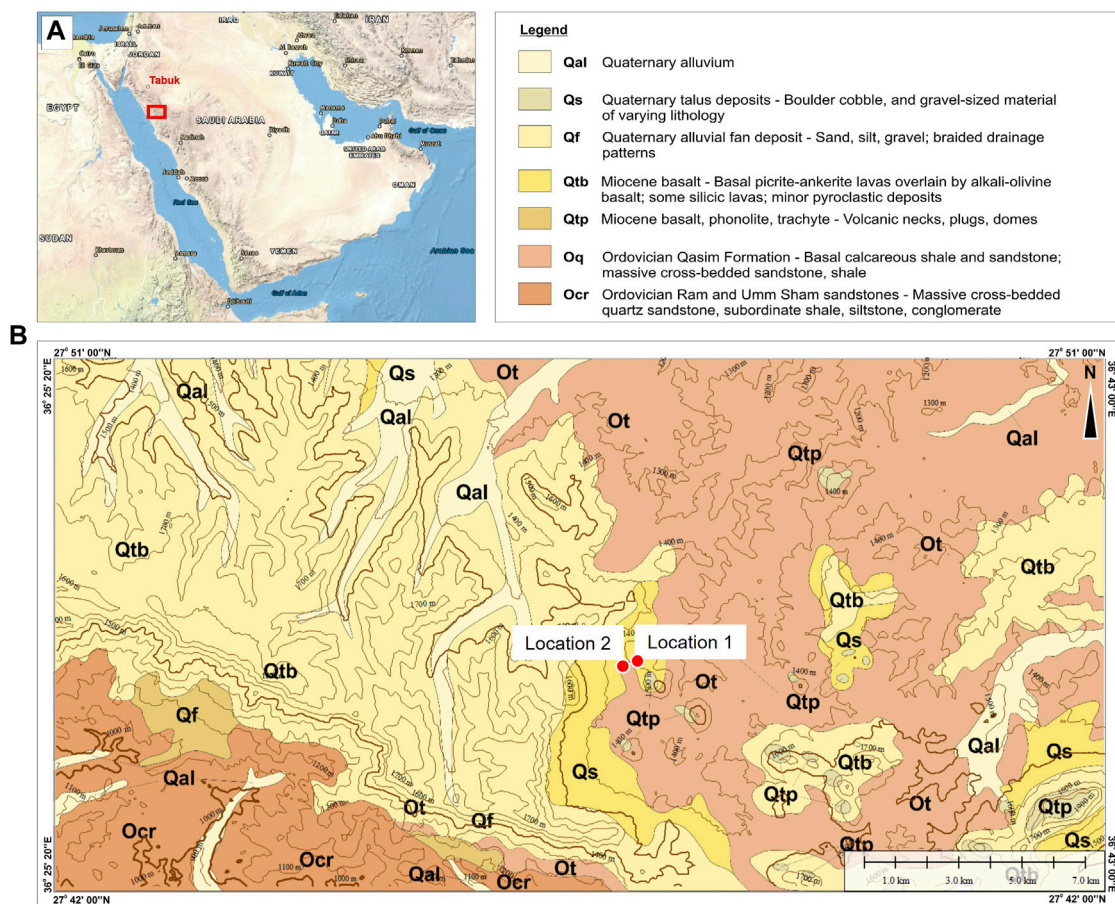


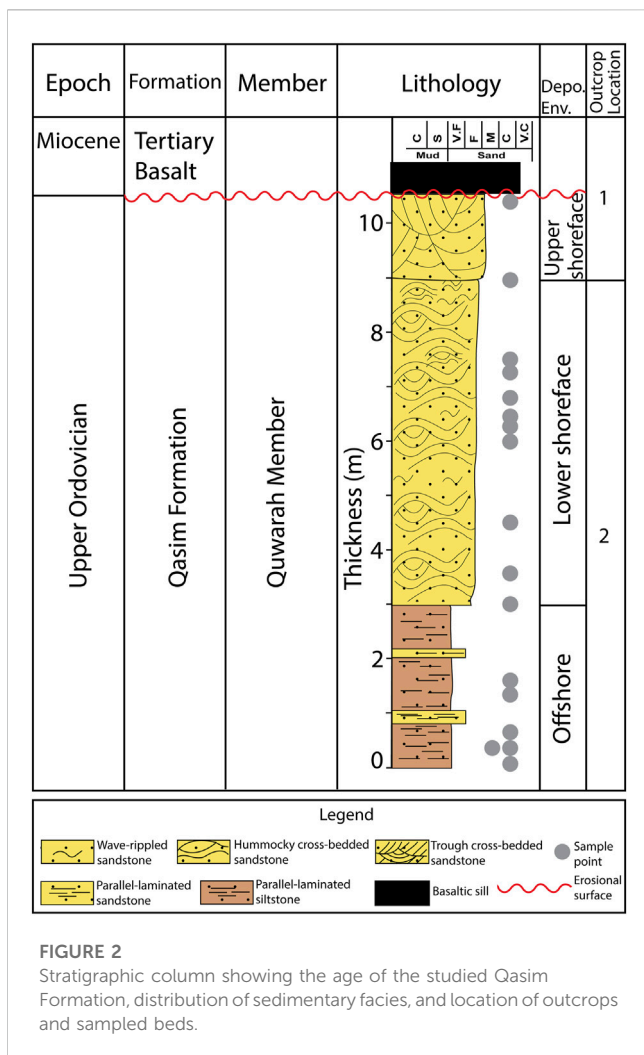
FIGURE 1
Location map of the study area. (A) Map of Saudi Arabia showing the study area (red box). (B) Simplified geological map showing the locations of the studied outcrops.

Formation has been described by [Manivit et al. \(1986\)](#) in the Buraydah quadrangle and by [Vaslet et al. \(1987\)](#) in the Baq'a quadrangle (Hail region). This formation has been interpreted to be deposited in shallow marine settings during tectonic quiescence ([Senalp and Al-Duaiji, 2001](#); [Laboun, 2010](#); [Craigie and Rees, 2016](#)). The lithology of the Qasim Formation comprises alternating cyclic units of thin-bedded, fine-grained sandstones to shale and thick-bedded, massive-to cross-bedded sandstones ([Powers et al., 1966](#)). These cyclic deposits were subsequently assigned as members of the Qasim Formation, consisting of the Hanadir (lower shale), Kahfah (lower sandstone), Ra'an (upper shale or siltstone) and Quwarah (upper sandstone) Members ([Powers et al., 1966](#); [Vaslet, 1990](#); [Senalp and Al-Duaiji, 2001](#); [Laboun, 2010](#); [Strother et al., 2015](#)). The studied samples were from the Quwarah Member of the Qasim Formation ([Figure 2](#)).

The Qasim Formation conformably overlies the continental, fluvial Saq Formation, with a thickness ranging from 261 to 358 m at the type locality and the northern Saudi Arabia ([Hussain and Abdullatif, 2004](#); [SGS, 2013](#)). The upward abrupt change in lithology suggests that the depositional environment shifted from continental to shallow- and deep-marine environments during the deposition of the lower, Hanadir Member of the Qasim Formation ([Sharland et al., 2001](#)). The depositional environment then switched back to shallow

marine, depositing the sandy Kahfah Member. Subsequently, the sequence was then repeated with the deposition of Ra'an Shale and Quwarah Sandstone Members ([Powers et al., 1966](#); [Senalp and Al-Duaiji, 2001](#)). The shaly Hanadir and Ra'an Members contain graptolites as diagnostic fossils indicative of deeper, low-energy open marine conditions whereas the sandy Kahfah Member contains *Skolithos*, indicating shallower, high-energy conditions ([Powers et al., 1966](#)). However, although diagnostic fossils were absent in the Quwarah Member ([McGillivray and Hussein, 1992](#)), *Skolithos* were identified as diagnostic fossil traces in pre-Tawil Sandstone, which is the lateral equivalent of the Quwarah Sandstone Member ([Powers et al., 1966](#)).

The study area experienced a gentle uplift and tilt following the deposition of the Quwarah Member, probably due to Taconic tectonic movements, resulting in a drop in sea level and the onset of glaciation ([Laboun, 2010](#)). Additionally, the Paleozoic successions, including the Qasim Formation, in the study area are overlain by Cenozoic volcanic rocks ([Grainger and Hanif, 1989](#)). Many faults have affected the Paleozoic rocks in the northeast of the Shaghab quadrangle (Map GM-109C; Sheet 27B), which were reactivated during the Tertiary due to the development of the Red Sea rift and resulted in the intrusion of



Tertiary mafic dikes into the fractures during the rift development (Grainger and Hanif, 1989).

3 Materials and methods

3.1 Field methodology

Detailed sedimentological log of the Quwarah Member of the Qasim Formation was constructed to capture bed thickness, lithology, color, grain size, sorting, sedimentary structures, types of bed contacts, and fossil content. The log was constructed for two, shallow stratigraphic sections, which were generally 400 m apart and about 10.5 m in total thickness (Figures 1B; Figure 2). The sections were selected based on the presence of basaltic sills, which directly overlie them. A total of 17 samples were collected in the measured sections (Figure 2).

3.2 Petrographic analysis

Seventeen (17) standard petrographic thin sections were prepared and impregnated with blue-dye resin for identification

of porosity. The thin sections were studied using an Olympus BX53F petrographic microscope. Point-count analysis was performed on the thin sections to determine the percentage of detrital framework grains, authigenic minerals, matrix content, primary and secondary porosities. The analysis was carried out using the Petrog software package, based on 300 counts per thin section. Grain size was measured by measuring the long axes of 100 fresh detrital quartz grains using the Petrog, at the end of which the average grain size and sorting were determined for each sample by the software.

3.3 XRD analysis

Bulk X-ray diffraction (XRD) analysis was conducted to complement the point-count data, scanning electron microscopy (SEM), and energy dispersive X-ray spectroscopy (EDS) analyses; to establish and quantify the sandstone constituents; and to guide the thin section analysis. The analysis was conducted at the Inorganic Geochemistry lab, College of Petroleum Engineering and Geoscience, King Fahd University of Petroleum and Minerals, Saudi Arabia. Prior to running the analysis, about 4 g of each sample was crushed, powdered using a Retsch RM 200 mill. The mill was cleaned with ethanol before and after each run. Powdered samples were prepared and loaded into sample holders with circular geometry and grooved shallow wells. XRD analysis was then carried out on all samples using Malvern PANalytical Empyrean Cu LFF HR diffractometer with Cu Kα1 radiation at a wavelength of 1.5406 Å and X-ray tube voltage and current set at 40 mA and 45 kV, respectively (Amao et al., 2022). Each bulk sample was scanned between 4° and 63° 2θ with a step size of 0.013° and scan step time of 8.67 s. However, to confirm the presence of dickite in some samples, the samples were scanned between 4° and 70° 2θ range. Qualitative analysis of all XRD data acquired was performed using the search-match module Highscore Plus software package (v. 4.9), with the reference database of ICDD PDF-4 2022. After the mineral phases were identified with Highscore Plus, they were further analyzed using the Rietveld quantitative XRD fitting tool.

3.4 Mineral identification using QEMSCAN®

An automated QEMSCAN® system was used for identifying and mapping of mineralogical composition of seven representative sandstone thin sections. In particular, the QEMSCAN technique was employed to establish the presence of chlorite and its relationship with kaolinite within intergranular pores. The instrument consists of Quanta 650 FEG scanning electron microscope (SEM) coupled with XFlash, Bruker Inc. energy-dispersive X-ray spectrometers (EDS). Before running the analysis, thin sections were carbon-coated using Q150T Quorum EMS 150R ES and then loaded into the QEMSCAN. The QEMSCAN analysis was conducted at the Center for Integrative Petroleum Research, King Fahd University of Petroleum and Minerals, Saudi Arabia. For this study, the QEMSCAN data were acquired using an X-Ray beam produced by accelerating voltage of 15 kV and a sample current of 10 nA (±0.05) (Amao et al., 2016). Field-scan mode was selected with a covered area of 1 cm² and 5 μm point spacing. The data was acquired and processed using iMeasure and iDiscover software packages, respectively.

TABLE 1 Petrographic point-count data.

	Min	Max	Average
Detrital Grains (%)			
Monocrystalline quartz	20	67	47.3
Polycrystalline quartz	0.0	0.0	0.0
Rock fragments	0.0	1.0	0.2
K-feldspar	0.0	0.7	0.1
Plagioclase	0.0	1.3	0.8
Biotite	0.0	2.0	0.2
Muscovite	0.0	6.0	0.7
Heavy minerals	0.0	0.7	0.0
Detrital matrix	0.0	0.5	0.0
Glauconite	0.0	0.3	0.0
Diagenetic minerals (%)			
Calcite	0.0	7.3	0.7
Hematite	0.3	18.0	6.7
Goethite	0.0	50.0	9.6
Grain-coating goethite/hematite	3.3	14.7	8.7
Ilmenite	0.0	9.4	1.1
Pyrite	0.0	0.3	0.1
Kaolinite	1.0	23.3	5.4
Chlorite	0.0	3.0	0.3
Grain-coating chlorite	0.0	0.7	0.0
Dickite	0.0	0.7	0.1
Quartz overgrowths	0.0	12.4	3.5
Porosity (%)			
Intergranular porosity	1.3	15.7	6.2
Opaque-lining intergranular porosity	0.0	15.6	7.7
Total intergranular porosity	3.0	25.0	13.9
Quartz-dissolution porosity	0.0	1.7	0.5
Cements (%)			
Total pore-filling cements	5.2	66.0	27.5
Total pore-filling goethite/hematite	0.6	58.3	17.5
Porosity loss (%)			
Compactional porosity loss (COPL)	8.8	31.2	18.9
Cementational porosity loss (CEPL)	3.6	21.9	12.8
Intergranular volume (IGV; %)	20.1	39.7	31.91
Textural parameters (mm)			
Mean grain size	0.3	1.0	0.5
Sorting (standard deviation)	0.1	0.5	0.2

3.5 SEM/SEM-EDS analysis

Stub samples were studied by scanning electron microscopy using Zeiss Gemini 500 scanning electron microscope equipped with an Aztec energy-dispersive spectrometer (EDS) and a backscattered electron detector (BSE), to identify minerals based on crystal morphological features, establish textural relationships between detrital grains and pore-filling materials, and determine

diagenetic features. The stub samples were coated with 10.0 nm platinum using a Leica EM 900, prior to running the SEM analysis. The SEM analysis was carried out at 5–15 kV voltage and current of 1–3 nA working conditions. The EDS analysis was performed using Aztec EDS (manufactured by Oxford Instruments, United Kingdom) and permitted mineral identification using spot chemical analysis to acquire semi-quantitative mineral composition.

4 Results

4.1 Mineralogy of the Qasim Formation

The studied Qasim sandstones are very fine-to medium-grained, with sorting ranging from moderately well-sorted to well sorted. Detrital grains are well-to very well-rounded. Quartz occurs as monocrystalline grains and ranges from 20% to 67% in abundance (Table 1). Detrital plagioclase prevails (trace to 1.3%) over K-feldspar (trace to 0.7%) (Table 1). Muscovite is the predominant mica (trace to 1.5%), whereas biotite occurs in trace amounts (<1%). Lithic fragments are mainly sedimentary in origin (trace to 1%). Glauconite and zircon are accessory minerals, with abundances generally $\leq 1\%$ each. Compositionally, the sandstones have been classified as mainly quartz arenites and rarely subarkoses (Figure 3), with an average, present-day composition $Q_{98}F_2L_0$, based on Folk (1980) classification scheme.

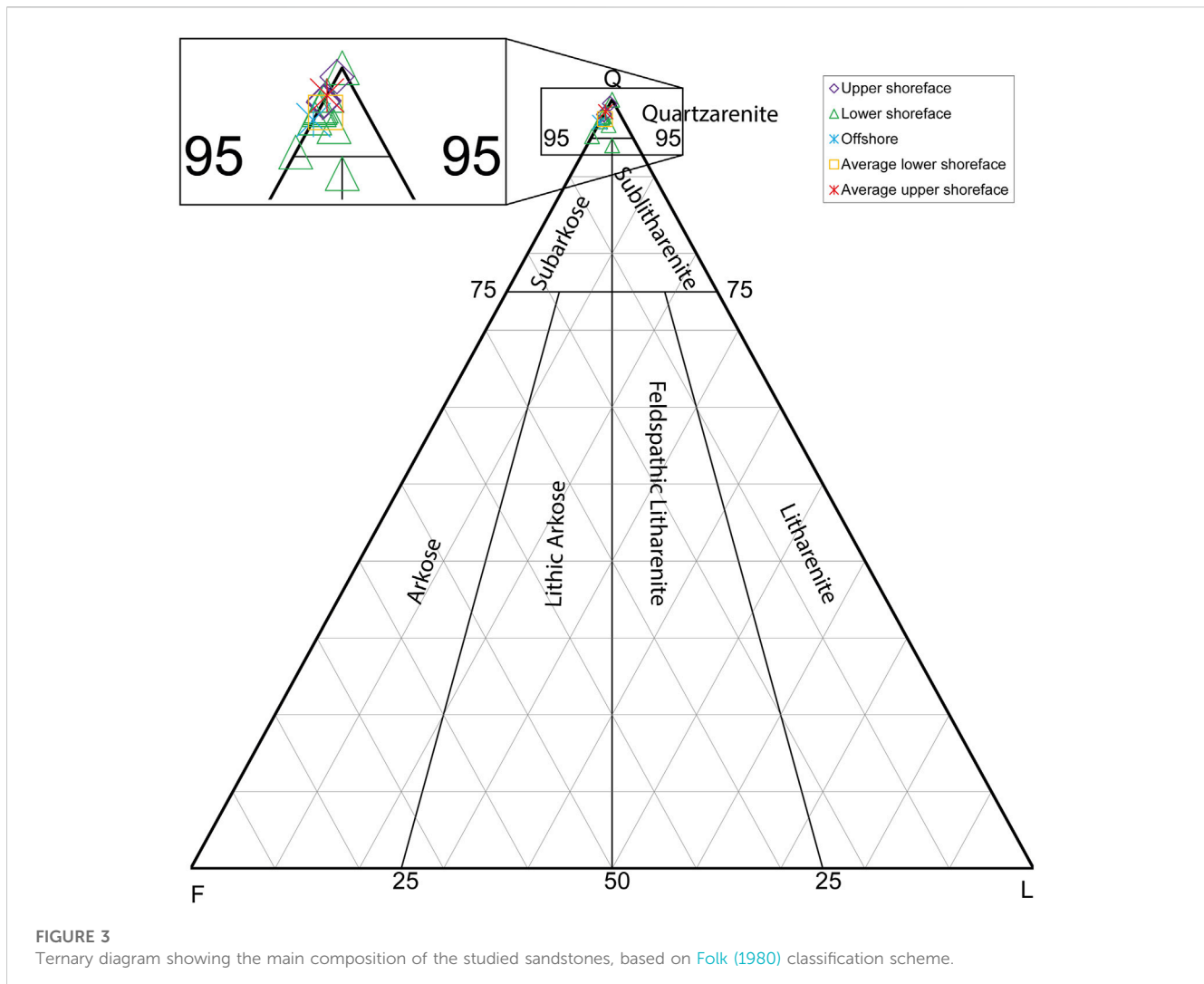
Results of the bulk XRD analysis show that detrital quartz is the main framework mineral in all samples (Figure 4). Kaolinite, dickite, calcite, goethite, biotite, and muscovite are the remaining predominant minerals (Figure 4), whereas hematite, ilmenite, and chlorite occur in very few to one samples (Table 2). The bulk XRD results show that the amount of quartz ranges from 47.5% to 99.2%, biotite from 0% to 2.8%, muscovite from 0% to 1.9%, kaolinite from 0% to 43.5%, dickite from 0% to 11.4%, calcite from 0% to 16.2%, goethite from 0% to 22.6%, hematite from 0% to 0.9%, ilmenite from 0% to 0.6%, garnet (andradite) from 0% to 1.4%, and chlorite from 0% to 0.8% (Table 2).

4.2 Sedimentology and depositional environments

Three main depositional facies have been established, including offshore, lower shoreface, and upper shoreface (Figures 5A–D). These depositional facies are overlain by basaltic sills (Figures 5E–G), which commonly range in thickness from 0.4 to 4 m and are relatively laterally extensive >300 m (Figure 5F). Sedimentary facies and interpretations.

4.2.1 Offshore (OS) facies

This facies consists of 3–4-m-thick, yellow to dark brown laminated siltstones (Figure 6A), forming the base of the studied section (Figures 5A, D). The OS facies comprises 29% of the studied sections. It transitions towards the top into an interbedded thin sandstone beds, which are very fine-grained and moderately well sorted. Additionally, the interbedded sandstones are often parallel-laminated and bioturbated sandstones. The parallel-laminated sandstones are laterally extensive (several tens of meters) and



range in thickness from 5 to 15 cm. This facies grades or sharply transitions upward into hummocky cross-stratified sandstones, forming a coarsening- and thickening-upward sequence.

This facies is interpreted to have been deposited in an offshore, low-energy depositional environment below the storm wave base (Senalp and Al-Duaiji, 2001; Sleveland et al., 2020).

4.2.2 Lower shoreface facies

This facies forms 57% of the studied outcrops, and consists of clean, fine- to very fine-grained, moderate to well-sorted sandstones, characterized by exhibiting hummocky cross-stratification (HCS) (Figure 6B). The HCS sandstones occur as upward thickening 5- to 30-cm-thick beds. They are laterally extensive (several tens of meters), and are often interbedded with very thin-laminated mudstones (Figure 5D). The interbedded mudstones and HCS sandstones form up to 1.5 m thick bed sets. They are commonly characterized by sharp, erosive bases. The erosional surfaces often contain pebble-sized rip-up mudstone clasts. The HCS sandstone beds grade into heavily bioturbated (*Skolithos*), wave-rippled sandstones (Figure 6C).

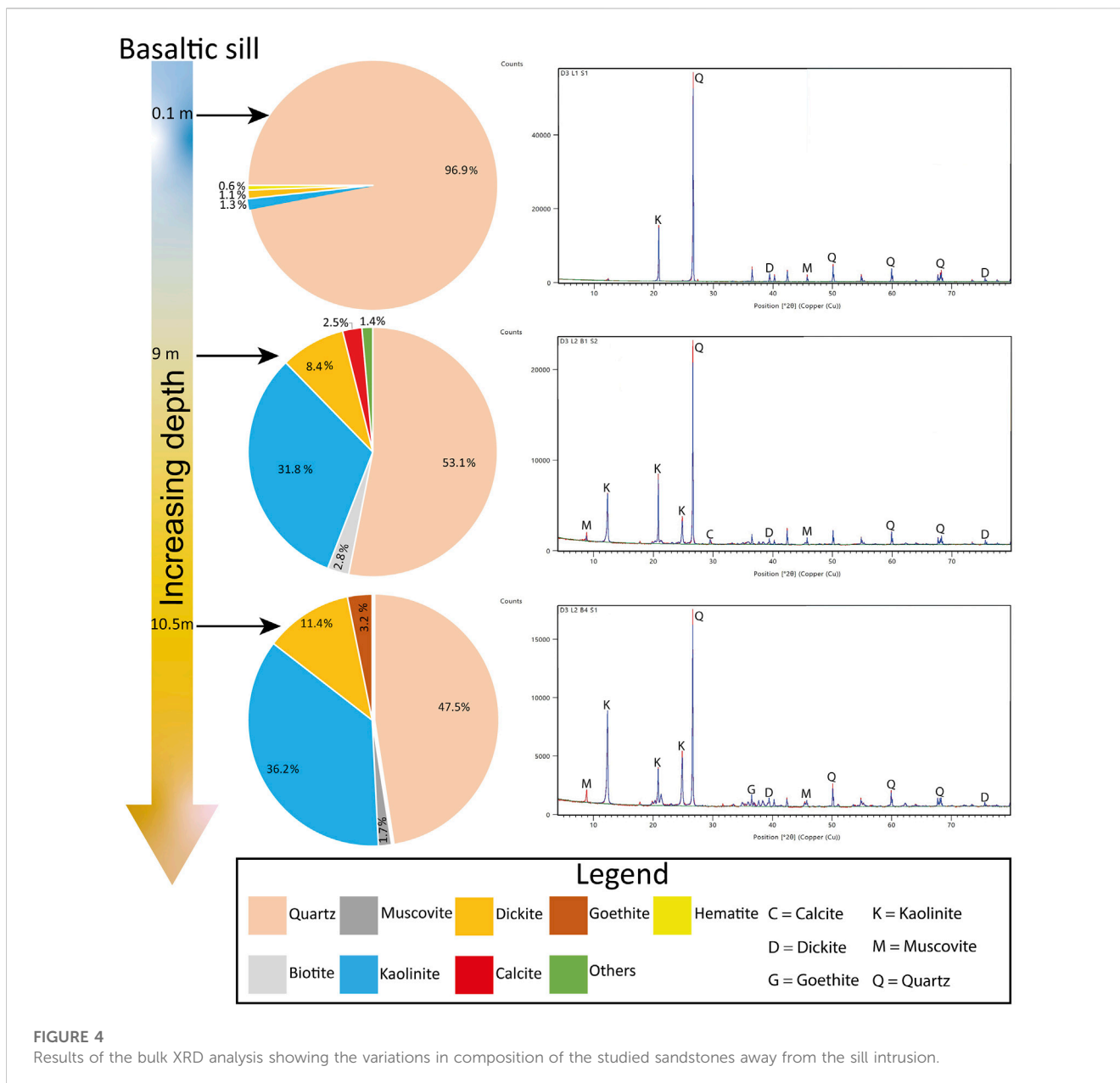
The HCS sandstones are widely interpreted to form by storm waves acting below the fair-weather wave base, with the

superimposed wave-ripple sandstones suggesting a combination of waning storm flows with combined storm wave action (Dott and Bourgeois, 1982; Swift et al., 1983; Walker et al., 1983). Therefore, these facies are interpreted to be deposited in a lower shoreface environment (Senalp and Al-Duaiji, 2001).

4.2.3 Upper shoreface facies

This facies consists of 1.5 m-thick bed of red to light brown, fine- to medium-grained, well-sorted, thinly bedded, and gently trough cross-bedded sandstones, which forms 14% of the studied outcrops of the Quwarah Member of Qasim Formation. The trough cross-bed sets range from 10 to 20 cm. They are often tigillite-burrowed. The facies constitutes the uppermost beds of the studied outcrops, and is in contact with the basaltic sill (Figure 5E; Figure 6D).

The trough cross-bedded sandstones are interpreted to indicate deposition above the fair-weather wave base in the upper shoreface depositional environment (Senalp and Al-Duaiji, 2001).



4.3 Diagenetic processes

4.3.1 Compaction

The most common types of grain contacts in the studied Qasim sandstones include floating, point, long, and concavo-convex grain contacts (Figures 7A–F). Mica grains, particularly muscovite, are generally flat (Figure 7E), with minor evidence of ductile deformation, slightly bending around detrital quartz grains (Figure 7F).

The impact of mechanical compaction on porosity loss has been evaluated following the criteria described by Lundegard. (1992) (Figure 8). The results show that compactional porosity loss (COPL) in the sandstones ranges from 8.8% to 31.2%, averaging 18.9% (Table 1). Additionally, the assessment of porosity loss due to cementation (CEPL) indicates that it ranges from 3.6% to 21.9%, averaging 12.8% (Table 1). Overall, porosity is lost mainly because of

compaction than because of cementation in the analyzed sandstones (Figure 8). Furthermore, the ICOMPACT (i.e., Compactional Index= COPL/COPL + CEPL) in the studied sandstones, according to Lundegard (1992), varies from 0.3 to 0.9, averaging 0.6. Additionally, ICOMPACT values of 0.0 and 1.0 indicate that all porosity loss is by cementation and compaction, respectively (Lundegard, 1992). Therefore, the average, ICOMPACT value of 0.6 for the studied sandstones further supports that compaction is the dominant diagenetic process through which porosity is reduced in the sandstones.

4.3.2 Cementation

4.3.2.1 Kaolinite

XRD analysis, SEM observations, and petrographic analysis reveal that kaolinite is the most abundant clay mineral present in the studied Qasim sandstones (Tables 1, 2). Results of the

TABLE 2 Bulk XRD results for the studied Qasim sandstones.

Sample code	Qtz (%)	Bio (%)	Mus (%)	Kao (%)	Dic (%)	Cal (%)	Hem (%)	Goe (%)	Ilm (%)	Oth (%)	Chl (%)	Total
B1	98.9	0.0	0.0	0.2	0.3	0.0	0.0	0.0	0.0	0.6	0.0	100
B1-2	53.1	2.8	0.0	31.8	8.4	2.5	0.0	0.0	0.0	1.4	0.0	100
B3	60.2	0.0	0.0	11.4	5.8	0.0	0.0	22.6	0.0	0.0	0.0	100
B4-1	62.0	1.9	0.0	18.8	0.0	0.0	0.0	17.4	0.0	0.0	0.0	100
B4-2	47.5	0.0	1.7	36.2	11.4	0.0	0.0	3.2	0.0	0.0	0.0	100
B4-3	48.7	0.0	1.9	43.5	2.4	0.0	0.0	3.5	0.0	0.0	0.0	100
B5	96.0	0.0	0.0	2.9	0.0	0.4	0.0	0.0	0.0	0.6	0.0	100
B6	83.3	1.2	0.0	15.3	0.0	0.0	0.0	0.0	0.0	0.3	0.0	100
B7	79.2	0.0	0.0	3.1	0.0	16.2	0.9	0.0	0.6	0.0	0.0	100
B8	88.8	0.0	0.0	10.3	0.0	0.4	0.5	0.0	0.0	0.0	0.0	100
B10	93.5	0.0	0.0	3.1	0.0	2.3	0.0	1.2	0.0	0.0	0.0	100
B11	94.6	0.0	1.4	3.0	0.0	0.7	0.0	0.0	0.0	0.3	0.0	100
B11-2	88.9	0.0	0.0	7.5	0.0	2.9	0.0	0.7	0.0	0.0	0.0	100
S1-1	93.6	0.0	0.0	1.9	3.5	0.0	0.1	0.0	0.0	0.0	0.8	100
S1-2	98.9	0.0	0.0	0.2	0.3	0.0	0.0	0.0	0.0	0.6	0.0	100
S1-3	96.9	0.0	0.0	1.3	1.1	0.0	0.6	0.0	0.0	0.1	0.0	100
S2	99.2	0.2	0.2	0.4	0.0	0.0	0.0	0.0	0.0	0.0	0.0	100
Min	47.5	0.0	0.0	0.2	0.0	0.0	0.0	0.0	0.0	0.0	0.0	100
Max	99.2	2.8	1.9	43.5	11.4	16.2	0.9	22.6	0.6	1.4	0.8	100
Average	81.4	0.4	0.3	11.2	2.0	1.5	0.1	2.9	0.0	0.2	0.0	100

petrographic point counting indicate that kaolinite varies from 1% to 23.3% (av. 5.4%) Kaolinite occurs in primary intergranular pores, and is found adjacent to or around altered (or leached) feldspar and mica grains (Figures 9A, B). The replacement of detrital mica by kaolinite occurs around bent muscovite grains between rigid framework grains (e.g., quartz) (Figure 9B). Additionally, kaolinite occurs adjacent to pervasively-dissolved feldspar grain (Figure 9C).

4.3.2.2 Dickite

Dickite is the second most abundant clay mineral in the studied sandstones (Table 2; Figures 9D–F). In addition, SEM observations reveal that dickite occurs in the vicinity of kaolinite, where the former replaces the latter (Figure 9E). Blocky dickites grew between partly dissolved, pseudo-hexagonal kaolinite crystals (Figures 9E, F).

4.3.2.3 Chlorite

Results of quantitative XRD analysis show that chlorite occurs in trace amount (0.8%) (Table 2). SEM analysis shows that chlorite is commonly associated with kaolinite and Fe-oxide minerals (Figures 10A–F). Additionally, chlorite replaces kaolinite in a pseudomorphic fashion (Figures 10A–C), where the chlorite inherits the crystal structure of the replaced kaolinite, but with differences in composition (lighter color due to Fe content). The

EDS analysis of the chlorite shows that it is Fe-rich (Figure 10D). Furthermore, SEM observations reveal that the rosette form of chlorite grew on and around dickite (Figure 10E). However, the replacement of kaolinite by chlorite was rarely observed on the dickite crystals (Figures 10C,E). Chlorite grew in the vicinity of dissolved Fe-oxide minerals (Figure 10F).

4.3.2.4 Quartz overgrowths

Quartz is one of the most common cements in the studied Qasim sandstones. It varies from 0% to 12.4% (av. 3.5%). The cement mainly occurs as overgrowths around detrital quartz grains. Optical microscopy reveals two types of quartz overgrowths: rounded and very angular (Figures 11A–D). However, while angular quartz overgrowths are common in the sandstones (Figures 11C,D), the rounded overgrowths dominate (Figures 11A,B). In both overgrowth types, nevertheless, their boundaries with detrital quartz grains are often delineated by dust rims or thin Fe-oxide coatings.

4.3.2.5 Oxide minerals

Petrographic observations and quantitative XRD analysis indicate that the oxide, opaque minerals consist of goethite, hematite, and ilmenite. However, goethite and hematite are the most abundant opaque minerals, with ilmenite being the least

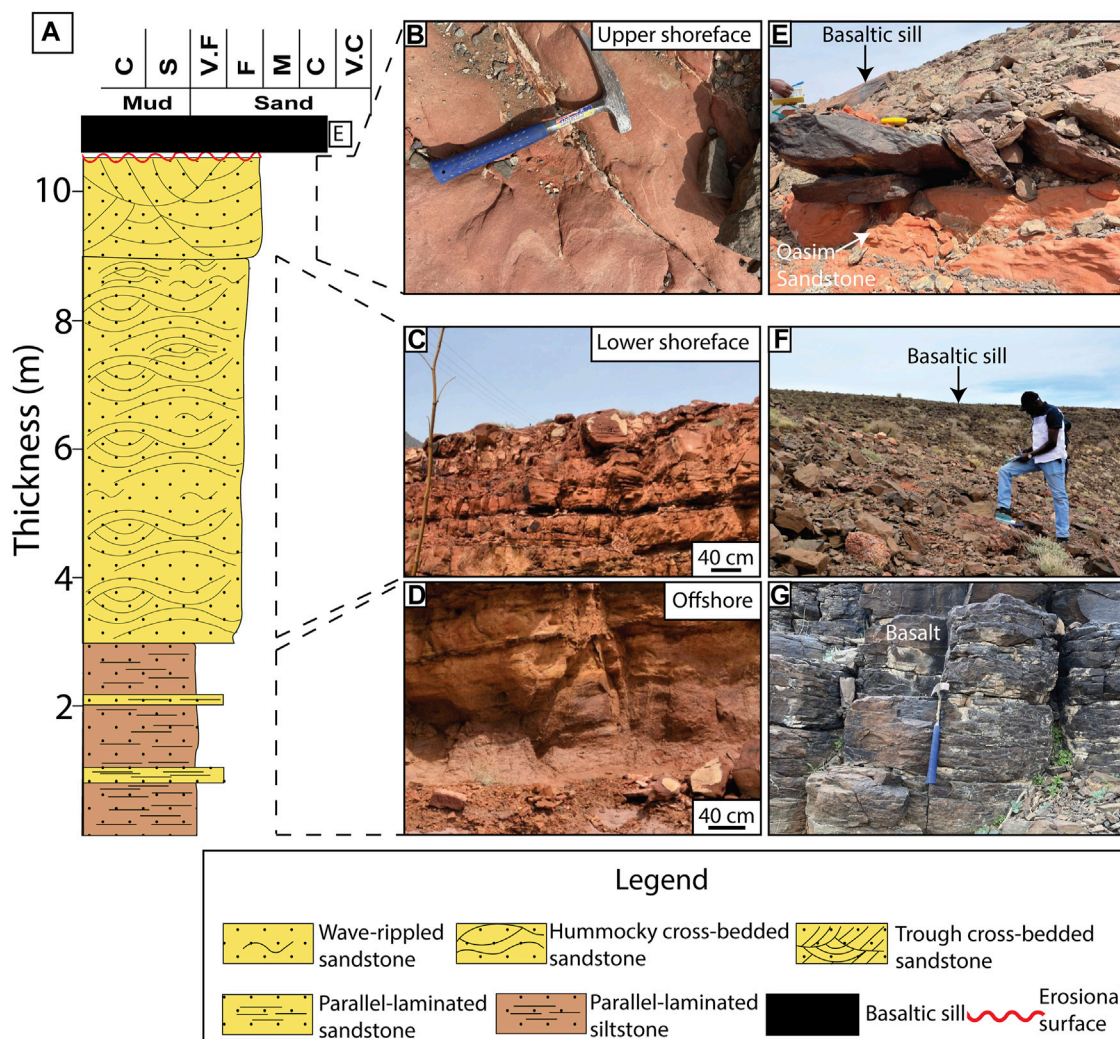


FIGURE 5 Sedimentary facies and interpreted depositional environments of the studied Qasim sandstones. (A) Stratigraphic log for the studied sandstones. (B) Upper shoreface facies (through cross bedded sandstone). (C) Lower shoreface facies. (D) Offshore facies. (E) Basaltic sill overlying the Qasim sandstone. (F) Laterally extensive basaltic sill. (G) Close-up view of the relatively thick basaltic sill (Location 1; see Figure 1B).

abundant and occurring in trace amounts (Table 2). While hematite and goethite occur as both grain-coating and pore-filling cements (Figures 12A–F), ilmenite mainly occurs as pore-filling cement. Point count data show that pore-filling goethite, hematite, and ilmenite vary from 0% to 50% (av. 9.6%), 0%–18% (av. 6.7%), and 0%–9.4% (av. 1.1%), respectively. Additionally, grain-coating opaque minerals range from 3.3% to 14.7% (av. 8.7%). Optical microscopy and SEM observations show that hematite exhibit rounded (Figures 12C, E) and needle-shaped morphologies (Figure 12D), whereas grain-coating goethite show bird-feather-type morphology (Figures 12E,F). In addition, the opaque minerals can also occur as pore-lining cements (Figure 12B).

4.3.2.6 Calcite

Calcite occurs mainly as a pore-filling cement (Figures 13A–F). Its abundance ranges from 0% to 7.3%, averaging 0.7%. Petrographic analysis reveals that the cement occurs between floating grains, and

encases well-rounded quartz overgrowths (Figure 13A). Additionally, it occurs as blocky, poikilotopic cement (Figure 13B), filling intergranular porosity. Two generations of calcite have been identified in the sandstones. The early or first-stage calcite was engulfed by kaolinite (Figure 13C) and hematite (Figure 13D). The late or second-stage calcite engulfed kaolinite (Figures 13E, F).

4.4 Magmatic-induced diagenesis

Thin-section optical microscopy and SEM analysis indicate that some minerals have undergone dissolution and replacements. For instance, detrital quartz has been partly and pervasively dissolved, creating secondary intragranular porosity (Figures 14A–C). In addition, the secondary intragranular porosities within detrital quartz are often filled by Fe-oxide cement (e.g., goethite; Figure 14A), dickite, kaolinite, and chlorite (Figures 14B, C). The

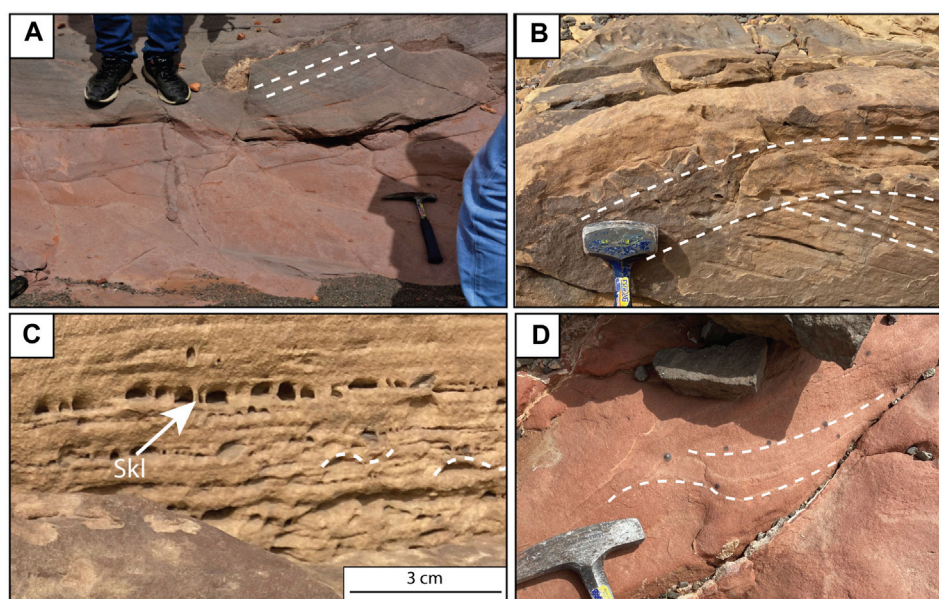


FIGURE 6

Close-up view of the established depositional facies. (A) Parallel-laminated siltstone. (B) Hummocky cross-stratified sandstone. (C) Wave-rippled sandstones with evidence of biotubations by *Skolithos* (*Skl*). (D) Trough cross-bedded sandstone.

dissolution of detrital quartz occurred in two forms: 1) dissolution restricted to the center of grains (Figures 14A, B); and 2) dissolution around the edges of detrital quartz (Figure 14D).

Furthermore, quartz overgrowths, notably the rounded ones, show major evidence of dissolution (Figure 14D). The overgrowths exhibit partial dissolution, breaking their continuity around detrital quartz grains and often creating embayments (Figure 14D). However, quartz overgrowths with angular, pointed edges show no evidence of dissolution in the analyzed sandstones (Figures 11C, D). In addition, intergranular, pore-filling calcite and goethite have undergone dissolution and create secondary intergranular porosity (Figures 14E, F).

4.5 Pore system

Two types of porosities were observed in the studied Qasim Formation, including primary, intergranular and secondary, intragranular porosities. The intergranular porosity is both opaque-mineral lined (Figures 12A, B) and non-opaque mineral lined, with percents ranging from 0% to 15.6% (average 7.7%) and 1.3%–15.7% (average 6.2%) (Table 1), respectively. Total intergranular porosity varies from 3% to 25% (average 13.9%; Table 1). Results of petrographic point count indicate that secondary porosity related to detrital quartz dissolution ranges from 0 to up to 1.7%, averaging 0.5%. However, because feldspars generally occur in trace amounts in the sandstones, SEM analysis has revealed that they often exhibit evidence of dissolution, with kaolinite replacing the altered grains (Figure 9C). Additionally, dissolved or altered mica grains (e.g., muscovite) show evidence of dissolution and replacement by kaolinite (Figures 9A, B). Thin section petrography shows that blocky kaolinite and dickite occur around altered muscovite (Figure 9A). Nevertheless, the secondary porosity created due to

calcite and goethite dissolutions (Figures 14E, F) are volumetrically insignificant, as they occur in trace amounts (<1% each).

4.6 Variation of minerals in relation to proximity to magmatic contact

The analyzed Qasim sandstones are overlain by a basaltic sill (Figures 5E–G), which ranges in thickness from 0.4 to 4 m. To investigate the role of the contact between the sill and sandstones on diagenesis, cross plots of diagenetic minerals in relation to the proximity to the sill contact have been constructed (Figures 15A–D). The results show that the amounts of authigenic kaolinite (Figure 15A) and dickite (Figure 4) increase away from the sill contact. However, the plot of quartz overgrowths against the distance below the sill contact shows that the cement relatively decreases away from the sill contact (Figure 15B). Additionally, the results show that while the volume of pore-lining Fe-oxide (Figure 15C) minerals increases towards the sill contact, pore-filling Fe-oxide minerals increase away from the sill contact (Figure 15D). Furthermore, values for compactional porosity loss have remained relatively similar at and away from the sill contact (Figure 15E). However, cementational porosity loss increases away from the sill contact (Figure 15F).

5 Discussion

5.1 "Normal" diagenesis

The types of grain-grain contacts and orientation of ductile grains (e.g., mica) can record the impact of mechanical compaction in sandstones (Figures 7A–F) (Chuhan et al., 2002; Al-Ramadan et al., 2013; Haile et al., 2019; Bello et al., 2021). While sandstones with

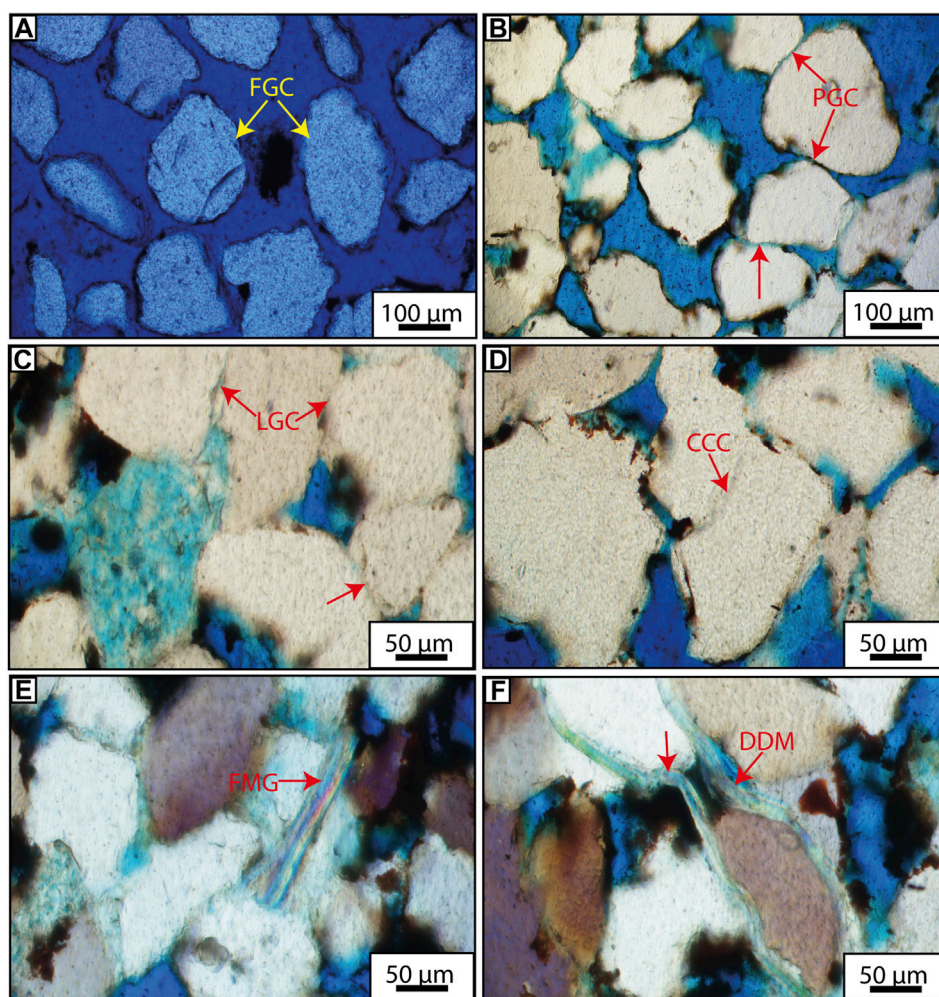


FIGURE 7

Thin-section photomicrographs indicating the extent of mechanical compaction in the studied sandstones. (A) Floating grain contact (FGC). (B) Point grain contact (PGC). (C) Long grain contact (LGC). (D) Concavo-convex contact (CCC). (E) Flat mica grain (FMG). (F) Ductile-deformed mica (DDM).

abundant sutured grain contacts indicate intense mechanical and chemical compaction, sandstones with floating, point and long grain contacts (Figures 7A–C) indicate a low degree of mechanical compaction (Heald, 1955; Haile et al., 2019). In the studied Qasim sandstones, the predominance of floating, point, and long grain contacts (Figures 7A–C) suggests that the sandstones have been subjected to little mechanical compaction, probably buried to a depth below 2 km before being uplifted. This is consistent with mica grains being flat to slightly deformed around detrital grains (Figure 7E, F). Concavo-convex contacts are very uncommon in the sandstones (Figure 7D). In addition, the Qasim sandstones in the Tabuk area are interpreted to have been uplifted following the deposition of the studied, sandy Quawarah Member of the Qasim Formation (Laboun, 2010), suggesting that the sandstones have undergone only shallow burial eodiagenesis (<2 km; <70 °C) (*sensu* Morad et al., 2010) before being exhumed and subjected to telodiagenesis (related to uplift). Furthermore, petrographic observations indicate that all diagenetic cements such as early calcite cementation (Figures 13A–C), kaolinite, feldspar, and mica dissolution show that the sandstones did not reach the quartz cementation window (>65°C) before being exhumed. The

observed quartz overgrowths with rounded edges (Figures 11A, B) suggest that they were not formed *in-situ* during burial and, hence, were most likely recycled or inherited (Sanderson, 1984; Hellevang et al., 2021), which resulted in the rounding of the edges of the overgrowths during transport. Consequently, all the above-mentioned suggest that the studied Qasim sandstones have been subjected to shallow burial, probably ≤ 2 km.

Most of the authigenic kaolinite occurs as a pore-filling cement, formed from alteration of feldspar and mica grains at shallow burial depth related to meteoric flushing either during shallow burial, eodiagenesis, or after uplift. Kaolinite is engulfed by goethite and hematite (Figure 14F), and therefore, they are interpreted to have formed during telodiagenesis related to uplift.

5.2 Evidence of magmatic-induced diagenesis

Magmatic intrusions can have impacts on the petrophysical properties of sandstone reservoirs and on the thermal maturation of

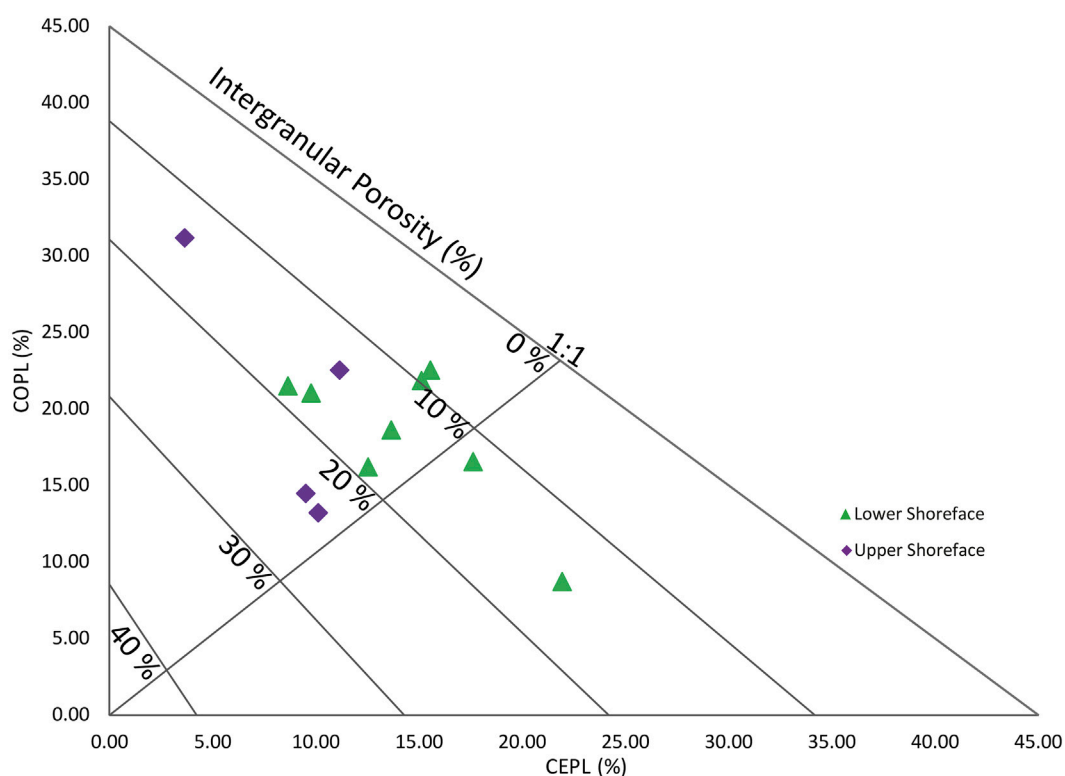


FIGURE 8

Plot of compactional porosity loss (COPL) against cementational porosity loss (CEPL) showing that compaction is the main driver for porosity loss in the studied sandstones.

hydrocarbon source rocks (Karlsen et al., 1998; Ochoa et al., 2007; Grove et al., 2017; Haile et al., 2019; Duffy et al., 2021; Rong et al., 2021). Geochemical reactions are often employed to understand the influence of magmatic systems in sedimentary basins characterized by anomalously high paleotemperatures compared to conventional burial history models (Ochoa et al., 2007). In this study, however, basaltic sill-induced diagenetic processes can be differentiated from normal diagenetic processes. This is because the Qasim sandstones in Tabuk region were only at shallow burial before their uplift (Laboun, 2010), and the diagenetic signatures in the studied sandstones indicate only shallow burial processes, except for those affected by quartz dissolution and conversion of kaolinite into dickite and chlorite.

5.2.1 Dissolution of detrital quartz

Unlike detrital feldspars and mica grains, which are chemically unstable during diagenesis, detrital quartz grains are chemically stable and, thus, are often less susceptible to chemical alteration during natural diagenesis (Bloch, 1994; Bello et al., 2021; Bello et al., 2022b). However, studies on the impact of magma-induced diagenesis on sandstones have shown that detrital quartz grains and authigenic quartz overgrowths can undergo dissolution due to magmatic intrusions (Haile et al., 2019; Rong et al., 2021). The dissolution of quartz grains has mostly affected the center of the detrital quartz grains (Figures 14A–C) and, rarely, the grain edges (Figure 14D). Nevertheless,

the dissolution of quartz overgrowths was only observed on rounded overgrowths (e.g., Figure 14D), suggesting that the overgrowths are most likely recycled and, hence, might have undergone long transport (Hellevang et al., 2021). Thus, the rounded overgrowths predate the pointed, angular quartz overgrowths (Figures 11A, B), which exhibit no evidence of dissolution and might have formed due to the intrusion. Consequently, the silica that has formed the angular quartz overgrowths might have been supplied from the dissolution of detrital quartz, feldspars, mica grains or transformation of clays (e.g., kaolinite to chlorite), which releases silica as by-product (Worden and Morad, 2003).

Previous studies have documented that the dissolution of quartz grains depends on the temperature and Ph value of the pore fluids in sandstones (Knauss and Wolery, 1988; Blake and Walter, 1999). For example, while the dissolution of quartz grains under alkaline solutions has been interpreted to occur at a temperature of over 130°C, those that occur under acidic solutions have been suggested occurring at a temperature of over 200°C (Zhang and Liu, 2014; Chen et al., 2015). The dissolution of detrital quartz in the studied sandstones might have occurred under acidic pore fluids, presumably supplied by the magmatic intrusion. This is because dickite and chlorite were found to fill the secondary dissolution pore within the quartz grains (e.g., Figure 14C), and the transformation of kaolinite into dickite is enhanced by an increase in the acidity of the formation waters (Worden and Morad, 2003).

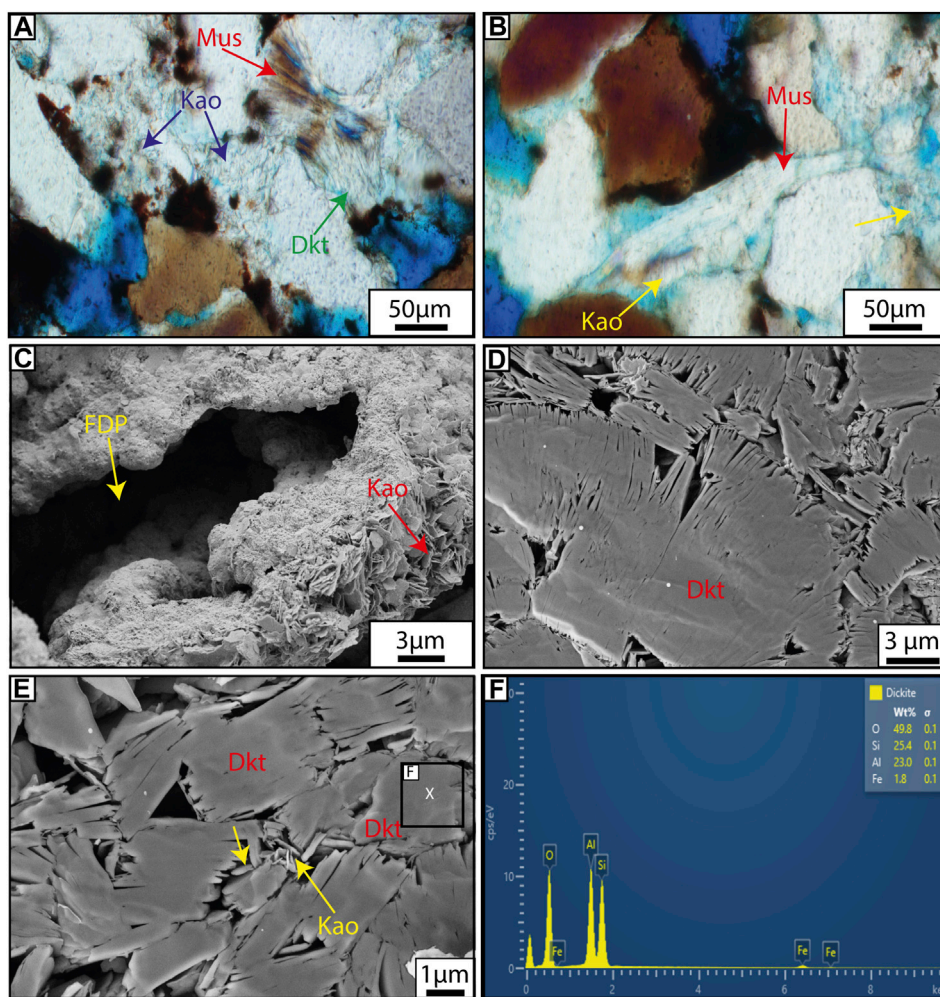


FIGURE 9

Thin-section photomicrographs and SEM images showing the mode of occurrence of kaolinite and dickite in the studied sandstones. (A) Kaolinite (Kao) growing around partly dissolved muscovite (Mus), and blocky dickite (Dkt) replaces the altered muscovite. (B) Authigenic kaolinite (Kao) replacing dissolved mica. (C) Kaolinite (Kao) occurring around feldspar-dissolution pore (FDP). (D) Blocky dickite (Dkt). (E) Blocky dickite (Dkt) and remnants of kaolinites (Kao). (F) Chemical composition of the dickite identified in (E).

5.2.2 Transformation of kaolinite into dickite

Kaolinite has been widely reported to transform into dickite with increasing burial depth and temperature (Morad et al., 1994; Lanson et al., 2002; Marfil et al., 2003; Worden and Morad, 2003; Bello et al., 2021). Although the transformation begins at a relatively shallow burial depth (2–3 km) and at a temperature ranging from 70 to 90°C, the ubiquitous, blocky transformation of kaolinite into dickite is believed to occur at 3–4.5 km burial depth and at a temperature varying from 90 to 130°C (Beaufort et al., 1998; Worden and Morad, 2003). This suggests that significant transformation of kaolinite into dickite takes place during deep-burial diagenesis (i.e., mesodiagenesis at a temperature >70°C) (Beaufort et al., 1998; Marfil et al., 2003; Worden and Morad, 2003). The transformation records the growth of monoclinic, blocky dickite between pervasively dissolved pseudo-hexagonal, vermiform kaolinite remnants, suggesting that the process proceeds in a dissolution-crystallization fashion (Figures 9D, E). However, like the transformation of smectite into illite, the conversion of kaolinite

into dickite has been found to occur over a prolonged period of time (Marfil et al., 2003), and in rocks characterized by high porosity and permeability (Lanson et al., 1996). In addition, Ehrenberg et al. (1993) and Morad et al. (1994) highlighted that the conversion of kaolinite into dickite is influenced by the type of the starting material, with the vermiform kaolinite (formed from feldspar dissolution) being more reactive than those from mica dissolution.

In the studied Qasim sandstones, dickite has grown between partly to pervasively dissolved pseudo-hexagonal crystals of kaolinite (Figure 9E) and, in most cases, the crystallization of dickite crystals significantly disrupts the stacking pattern of the kaolinite (Figure 9D). This is presumably because the transformation seldom goes to completion, thereby distorting the stacking pattern (Worden and Morad, 2003). However, petrographic and SEM analyses of the studied Qasim Formation show that there is no evidence of deep-burial diagenetic processes such as tight packing and presence of deep-burial, mesogenetic illite, suggesting that the transformation of kaolinite into dickite might have been influenced

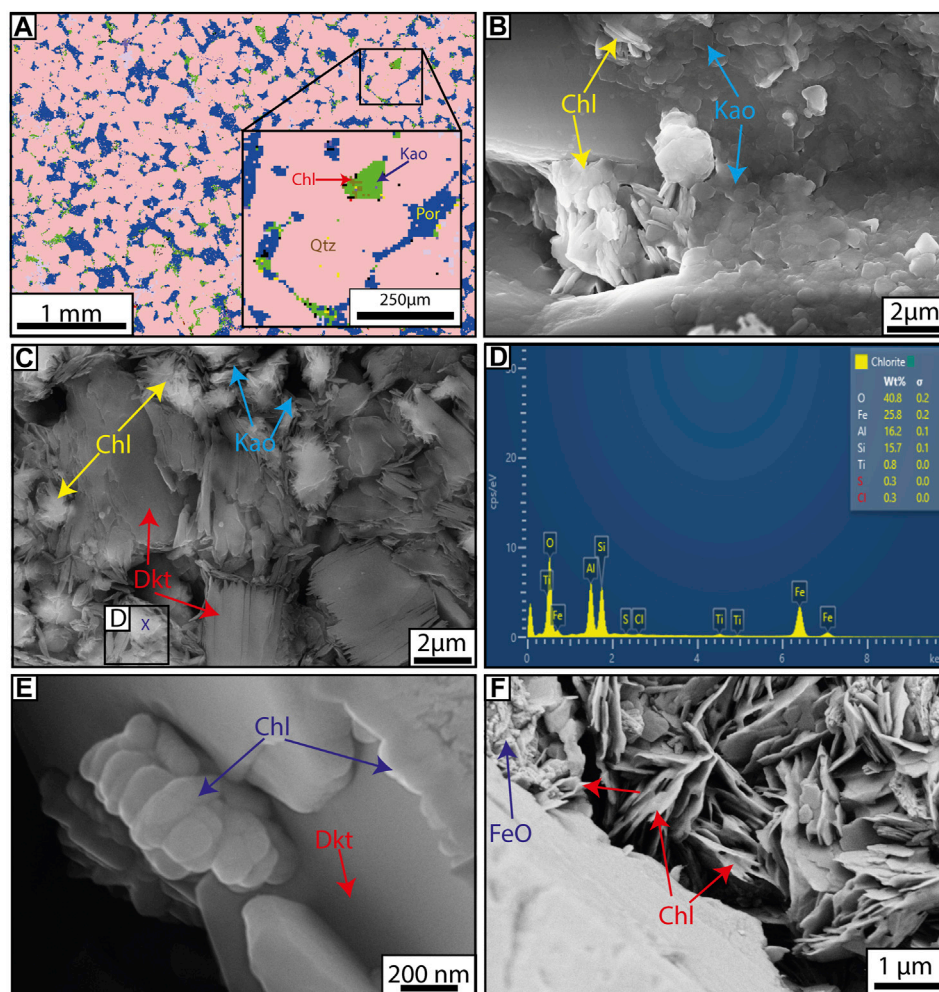


FIGURE 10

Mode of occurrence and morphologies of chlorite in the sandstones. (A) QEMSCAN image showing close association between kaolinite (Kao) and chlorite (Chl). They grow between detrital quartz (Qtz) and within the pore (Por). (B) Chlorite (Chl) replacing the disrupted crystals of kaolinite (Kao). (C) Chlorite (Chl) replacing kaolinite crystals, with dickite (Dkt) remaining completely unreplaced. (D) EDS analysis of the identified chlorite in (C). (E) Rosette chlorite (Chl) growing on dickite (Dkt). (F) Chlorite (Chl) occurring between dissolved FeO minerals.

by the magmatic flow. This implies that the magmatic intrusion might have created the acidic conditions required for the transformation, and the transformation was probably enhanced by the porous and permeable nature of the sandstones (Figures 7A, B) (Beaufort et al., 1998; Worden and Morad, 2003). Additionally, the transformation of kaolinite into dickite has been linked to acidic pore fluid generated from the maturation of hydrocarbon source rocks (Marfil et al., 2003). However, given the substantial burial depths at which the maturation of source rocks and the transformation of kaolinite into dickite occur, it is implausible that the dickite in the Qasim sandstones were formed during source rock maturation as well as deep-burial diagenesis. Instead, we interpret that the dickite was formed from acidic pore fluids supplied by magmatic intrusion. Furthermore, the observed disrupted stacking pattern of pseudo-hexagonal crystals of kaolinite around dickite suggests that, although the magmatic intrusion has provided the required acidic conditions as well as the temperature, the duration of the exposure to the required temperature for the

transformation was probably not long enough to drive the reaction to completion. Moreover, calcite has been reported as a by-product of the transformation of kaolinite into dickite (Worden and Morad, 2003). Consequently, in the analyzed Qasim samples, late calcite was observed to engulf kaolinite and, therefore, postdates it (Figures 13E, F).

In the studied Qasim sandstones, the transformation of kaolinite into dickite occurred in preference to the transformation of kaolinite into illite chiefly because of two main reasons. First, the quartz-rich nature of the sandstones suggests that sufficient K-feldspar is lacking, and K-feldspar supplies the required K^+ for illitization of kaolinite to occur at a temperature $>120^\circ\text{C}$ (Bjørlykke et al., 1995). The lack of K-feldspar content, therefore, would favor the formation of dickite instead of illite. Second, the small K-feldspar content might have been completely dissolved and the K^+ transported elsewhere prior to the illitization process. In addition, almost all the observed kaolinite (and dickite) occurs around altered, detrital muscovite,

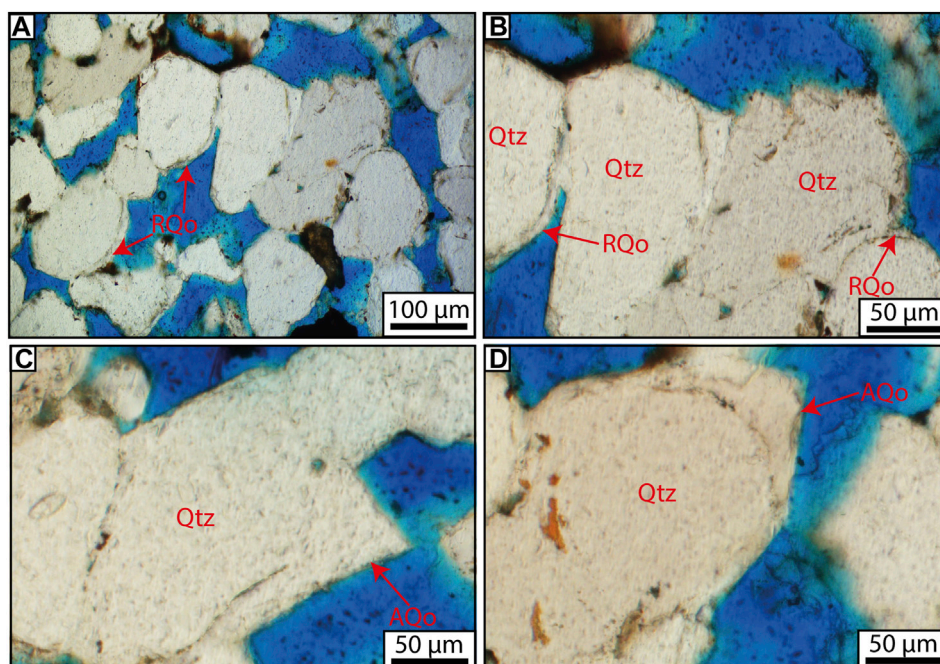


FIGURE 11

Thin-section photomicrographs showing the types of quartz overgrowths in the sandstones. (A, B) Rounded quartz overgrowths (RQo) occurring around detrital quartz grains. (C, D) Angular quartz overgrowths (AQo) occurring on detrital quartz grains.

indicating that the observed muscovite was the main precursor for the authigenic kaolinite in the sandstones (Figures 9A, B).

5.2.3 Transformation of kaolinite into chlorite

Kaolinite and smectite are reported to transform into chlorite under highly acidic conditions and high Fe content (Chen et al., 2011). Additionally, the transformation of kaolinite to chlorite is a function of burial depth and temperature (Moraes and De Ros, 1992). Boles and Franks (1979) reported that the conversion of kaolinite to chlorite occurs at burial depths ranging from 3.5 to 4.5 km and at a diagenetic temperature ranging from 165 to 200°C. However, for the studied Qasim sandstones, based on our petrographic data and previous study (e.g., Laboun, 2010), it is highly unlikely that the sandstones attained a 3.5 km burial depth and a minimum threshold temperature of 165°C before being exhumed. Thus, the chlorite associated with kaolinite (and sometimes dickites) in the sandstones was probably formed due to the impact of magmatic intrusion. This is corroborated by the presence of dickite and chlorite in the secondary porosity within detrital quartz grains, created presumably due to the magmatic influx in the sandstones (Figures 14B, C).

Although the high Fe content required for the transformation of smectite and kaolinite to chlorite is often supplied by volcanic rock fragments, siderite, and ankerite (Worden and Morad, 2003; Chen et al., 2011; Bahlis and de Ros, 2013; Worden et al., 2020), our XRD and SEM-EDS data indicate that such minerals are absent in the Qasim sandstones. In contrast, the studied sandstones are characterized by high hematite and goethite contents, which could potentially supply the requisite high Fe content for the transformation to occur. Nevertheless, the process probably

requires Fe to be dissolved, transported, and incorporated into the kaolinite crystal structures. A study on the chemical stability of goethite and hematite (Berner, 1969) reports that goethite is more chemically unstable than hematite and, therefore, tends to dissolve at a temperature of 85°C. Our SEM analysis shows that goethite displays evidence of dissolution (Figure 14F), which is absent in hematite. Additionally, goethite engulfs kaolinite (Figure 14F) and, thus, postdates it and formed very likely during late diagenesis related to uplift. As a result, the goethite is hereby interpreted to have supplied the high Fe content required for the transformation of kaolinite to chlorite. Additionally, the magmatic intrusion might have dissolved and transported the Fe from goethite to the sites of kaolinite as well as have provided the required temperature and the high acidic conditions. Furthermore, goethite has been found to occur in the vicinity of chloritized kaolinite (e.g., Figure 10F) in the sandstones. Nonetheless, kaolinite was observed to be more susceptible to chloritization than dickite (Figures 10B, C), as reported by Worden and Morad (2003).

5.3 Paragenetic sequence for burial-, uplift- and magmatic-related diagenesis

The establishment of paragenetic sequence is crucial for understanding the sequence of diagenetic events that affect sandstone reservoirs, which can significantly improve their reservoir quality prediction. In the studied sandstones, the formation of calcite, pyrite, and kaolinite cements and mechanical compaction are considered as the earliest diagenetic processes that affected the sandstones (Figure 16; Figure 17), which

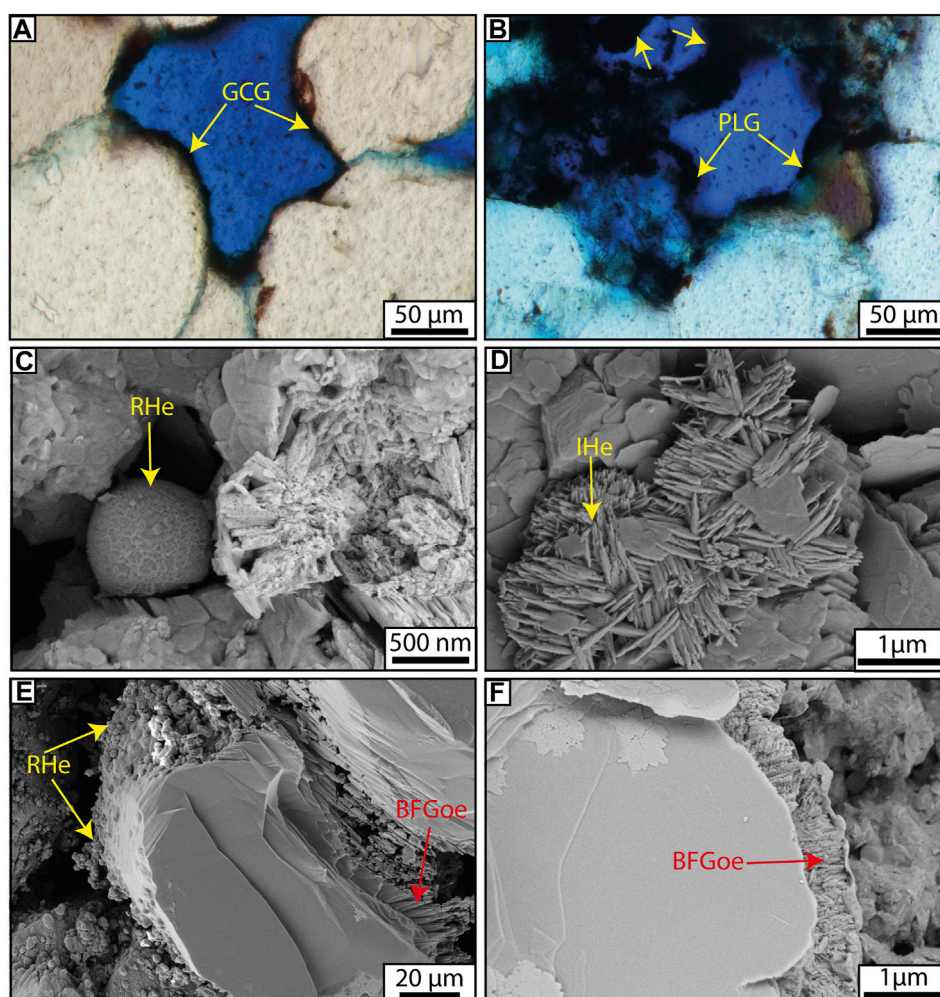


FIGURE 12

Thin-section photomicrographs and SEM images showing the mode of occurrence of Fe-oxide minerals. (A) Grain-coating goethite (GCG). (B) Pore-lining goethite (PLG). (C) Rounded hematite (RHe). (D) Iridescent hematite (IHe) occurring as needle-shaped. (E) Rounded hematite (RHe) engulfing bird-feather goethite (BFGoe). (F) Bird-feather goethite (BFGoe) occurring as grain-coating cement around detrital quartz.

occurred during eodiagenesis and presumably at a temperature of <70 and burial depth of <2 km. Early calcite occurs in sediments with loose packing and floating grain contacts (Figure 13A) and often occurs as poikilotopic cement (Figure 13B). The origin of the early, poikilotopic calcite in marine sandstones has been linked to recrystallization from skeletal debris, which serve as substrates and nucleation sites for calcite cement to precipitate (Hakimi et al., 2012). Framboidal pyrite forms from microbial sulfate reduction near sediment-water interface. However, the framboidal pyrite in the Qasim sandstones has probably been completely oxidized and replaced by rounded hematite during the uplift-related diagenesis (Figure 12C & 17) (Grove et al., 2017). Eogenetic kaolinite occurs around partly or pervasively dissolved muscovite grains (Figures 9A, B; Figure 17), and was formed probably due to meteoric flushing during sea-level low-stands and progradation of shallow marine sands (Morad et al., 2000; Ketzner et al., 2003). Eogenetic kaolinite engulfs and, thus, postdates the early diagenetic calcite (Figure 13C).

Telogenetic alterations related to uplift in the studied sandstones include the dissolution of early calcite formation of goethite, kaolinite, goethite, and hematite. Early calcite in the studied Qasim sandstones has undergone dissolution (Figure 14E), presumably due to the influx of acidic, meteoric fluid during the uplift, creating secondary intergranular porosity within the calcite (Figure 14E). However, it is unclear whether the dissolution of the early calcite was related to percolation of CO₂-rich fluid from the magmatic source. Additionally, authigenic kaolinite continued to form during the uplift probably due to meteoric flushing or the influx of CO₂-rich fluid from magmatic intrusions. This is corroborated by the presence of kaolinite, which has transformed into dickite and chlorite, within the dissolved detrital quartz grains (Figure 14C). Goethite and hematite are important Fe-rich minerals that form under oxidizing conditions (Berner, 1969; Chan et al., 2000; Busigny and Dauphas, 2007). The mixing of Fe-rich fluid, probably during the uplift, with oxidizing groundwater has resulted in the precipitation of goethite and hematite (Chan et al., 2000; Busigny and Dauphas, 2007). However, in the analyzed sandstones,

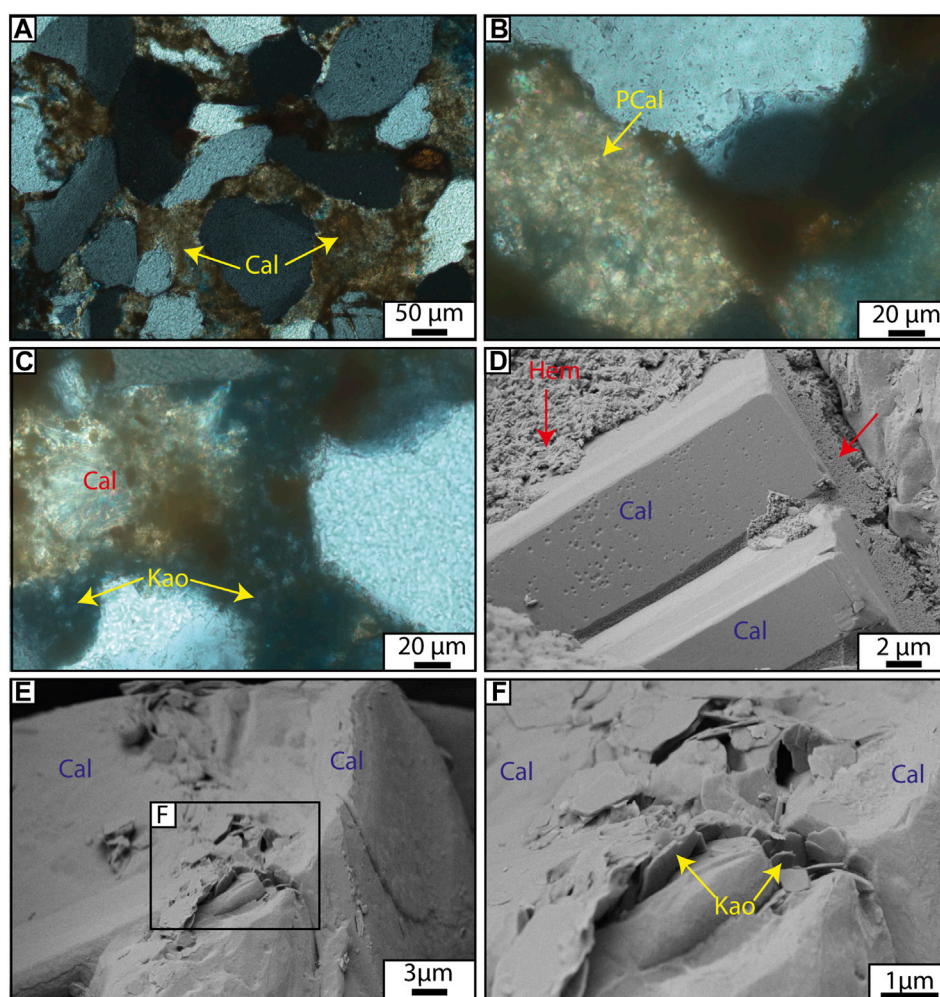


FIGURE 13

Petrographic relationship between calcite and other minerals. (A) Calcite (Cal) occurring between floating grains. (B) Poikilotopic calcite (PCal) blocking intergranular porosity. (C) Kaolinite (Kao) engulfing early-stage calcite. (D) Hematite (Hem) engulfing early-stage calcite. (E) Late-stage calcite (Cal) engulfing kaolinite (Kao). (F) Close-up image of (E) showing late-stage calcite (Cal) engulfing kaolinite (Kao).

rounded hematite was observed to engulf goethite, indicating that it postdates the goethite (Figure 14F). This is probably because the hematite was formed from the dehydration of goethite, as the latter is chemically unstable relative to the former (Berner, 1969).

The formation and distribution of magmatic-related diagenetic minerals within pore networks is strongly influenced by the type of diagenetic minerals prior to the magmatic intrusion (Mckinley et al., 2001). Therefore, understanding the “normal” diagenetic mineralogy is crucial to understanding the heating effects on the sandstones. The earliest diagenetic mineral related to the heating effect on the sandstone was dickite (Figure 14C; Figure 17). The dickite engulfs crystals of kaolinite, indicating that it was formed after the formation of kaolinite. As stated above, petrographic data and SEM analysis suggest that the sandstones have experienced shallow burial diagenesis, with depths and temperatures too shallow and low, respectively, to form dickite through normal diagenesis. While pseudomorphic chlorite, which replaces kaolinite, grows between dickite crystals (Figures 10B,C), rosette chlorite engulfs

dickite (Figure 10E), suggesting that the conversions of kaolinite into chlorite and dickite occurred at the same or similar time.

5.4 Implications for reservoir quality

The injection of magmatic fluids into cooler sandstone reservoirs can have significant impacts on porosity (Einsele et al., 1980; Senger et al., 2014; Sydnes et al., 2019b; Haile et al., 2019). The extent of magmatic sill-induced diagenetic alterations in sandstones largely depends on their proximity to the sill, the thickness of the sill, the depth at which the sill intrusions occur, and the clusters of the sill (Aarnes et al., 2011; Sydnes et al., 2019b; 2019a; Chen et al., 2021). Previous studies on the role of magmatic intrusions on sandstones porosity evolution and diagenesis have come to contrasting conclusions of both positive and negative impacts on porosity (Feng and Tang, 1997; Mckinley et al., 2001; Grove et al., 2017; Chen et al., 2021). In the present study, intergranular porosity

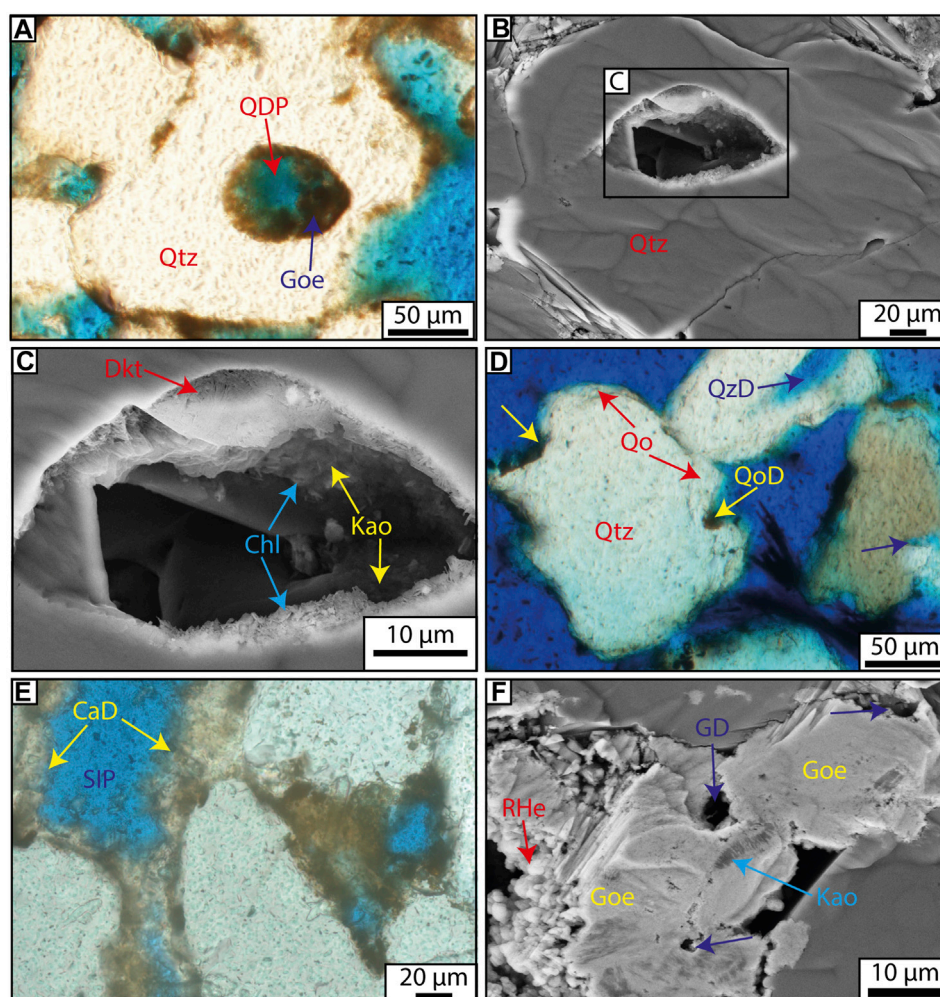


FIGURE 14

Photomicrographs showing mineral dissolutions and replacements. (A) Quartz (Qtz) dissolution pore (QDP) being filled by goethite (Goe). (B) Dissolution of quartz grain around the center of the grain. (C) Inset of (B) showing secondary-dissolution pore in quartz being filled by dickite (Dkt), chlorite (Chl) and kaolinite (Kao). (D) Quartz dissolution (QzD) around grain edges and dissolution (QoD) of quartz overgrowths (Qo), creating embayments on the grain. (E) Early calcite undergoing pervasive dissolution (CaD) and creating secondary intergranular porosity (SIP). (F) Goethite (Goe) undergoing dissolution (GD) and replacement by rounded hematite (RHe). Note how goethite engulfs kaolinite (Kao).

decreases away from the magmatic sill contact (Figure 18A). This can be attributed to three factors: (1) primary depositional controls (e.g., grain size and sorting); (2) diagenetic controls; and (3) impact of magmatic intrusions. Sandstones with coarser grain size tend to have better sorting, and porosity increases with increasing grain size and better sorting (Figures 18B,C). Intergranular porosity increases with increasing volume of grain-coating Fe-oxide (Figure 18B). However, it could not be established whether or not the grain-coating Fe-oxide cements have inhibited quartz cementation. This is mainly because the quartz overgrowths might have been predominantly inherited, as they are well rounded (Figures 11A, B).

Additionally, pore-filling kaolinite is one of the major cements that has negatively affected the intergranular porosity of the sandstones (Figure 16; Figure 17; Figure 18E), and kaolinite increases in volume away from the sill contact (Figure 15A). This is because most of the kaolinite is associated with muscovite grains. Due to their grain shape, low density, and hydrodynamic processes,

mica grains (e.g., muscovite) are deposited in low-energy environments (e.g., offshore) (Mansurbeg et al., 2008; Marchand et al., 2015; Bello et al., 2021). Thus, kaolinite could form in sandstones in close proximity to offshore environment, resulting in the occlusion of intergranular porosity if meteoric flushing occurred. Additionally, XRD data show that dickite increases away from the sill contact (Figure 4). This is probably because: 1) the dickite is strongly associated with muscovite grains and kaolinite; and 2) there could be another heat source below the studied outcrops (i.e., sill or dike) (Figure 17), which might have supplied sufficient heat for the conversion of kaolinite into dickite. Based on XRD, SEM, and QEMSCAN analyses, chlorite was only observed in few sandstone samples and, therefore, its occurrence is localized. As a result, it might have less impact on the intergranular porosity of the sandstones. Pore-filling opaque minerals, mainly consisting of goethite and hematite, have negatively impacted the intergranular porosity of the sandstones (Figure 18F), and their

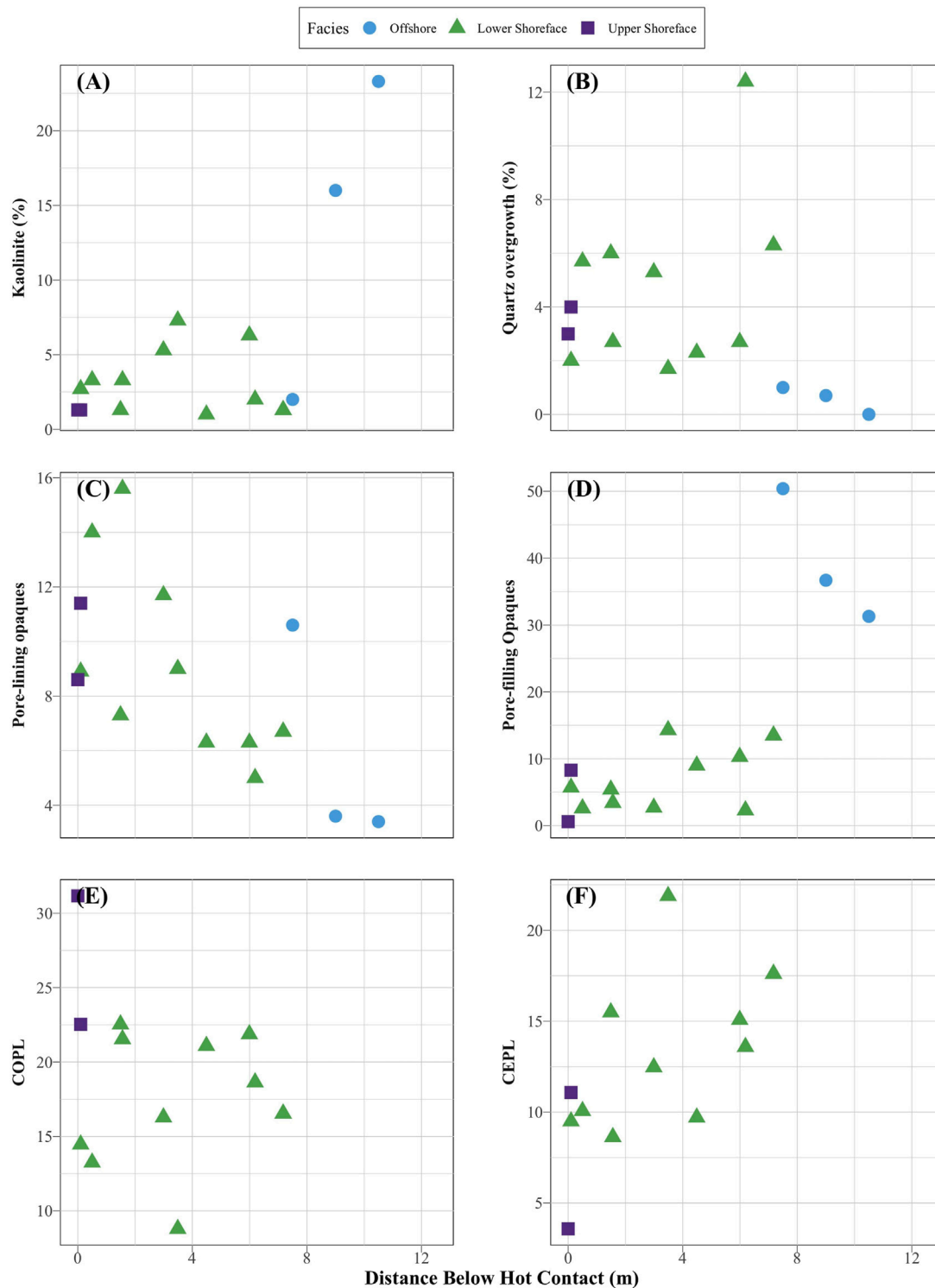


FIGURE 15

Variation of diagenetic minerals in relation to the distance from sill contact. **(A)** An increase in kaolinite content away from the sill contact. **(B)** Plot of quartz overgrowths against distance from the sill showing a decrease in abundance of quartz overgrowths away from the sill contact. **(C)** Decrease in pore-lining Fe-oxide minerals away from the sill contact. **(D)** Increase in pore-filling opaque minerals (FeO) away from the sill. **(E)** Plot of compactional porosity loss (COPL) against distance below the sill contact showing relatively stable compactional porosity loss away from the sill contact. **(F)** Plot of cementational porosity loss (CEPL) against distance below the sill contact showing an increase in cementational porosity loss away from the contact.

Diagenetic Minerals & Alterations	Shallow Burial (Eodiagenesis)	Uplift (Telodiagenesis)	Intrusion-induced Diagenesis	Effect on Porosity	
				-ve	+ve
Pyrite	██████			██████	
Hematite		██████		██████	
Early calcite	██████			██████	
Calcite dissolution		██████	██████?		██████
Feldspar & mica dissolution	██████	██████	██████?		██████
Kaolinite	██████	██████	██████?	██████	
Dickite			██████	██████	
Chlorite			██████	██████	
Quartz dissolution			██████		██████
Quartz overgrowth (angular)			██████	██████	
Goethite		██████		██████	
Late calcite			██████?	██████	
Mechanical compaction	██████			██████	

FIGURE 16 Paragenetic sequence of diagenetic events in the Qasim sandstones and their overall positive (+ve) and negative (-ve) impacts on porosity.

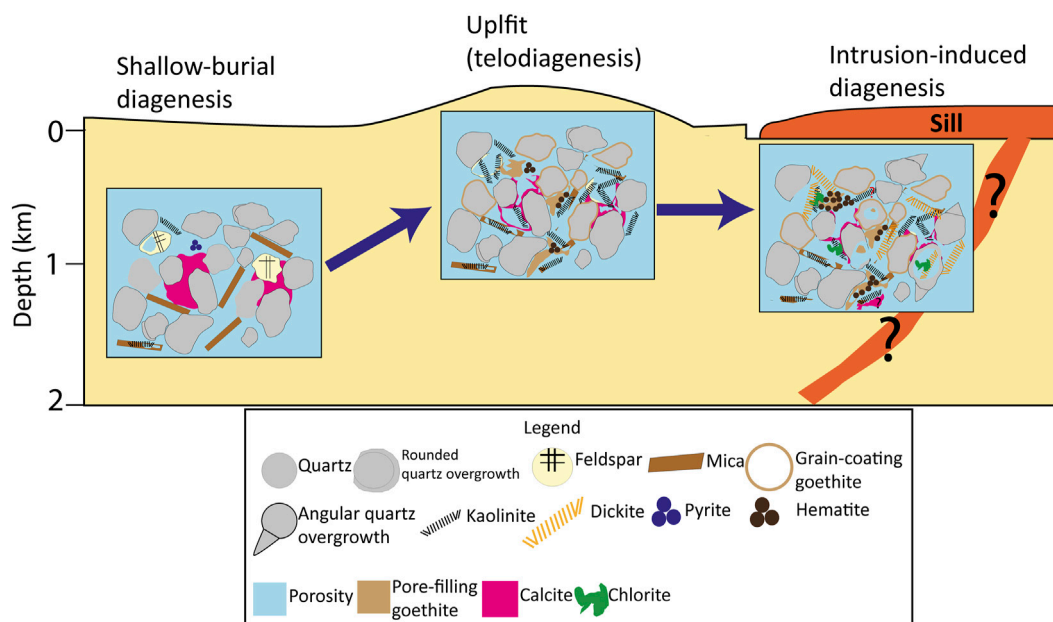


FIGURE 17 Conceptual model for the diagenetic processes in the studied Qasim sandstones.

volume percent increases away from the sill contact (Figure 15D). This is presumably because of the close proximity with Fe-rich oxidizing groundwater that facilitate their formation.

The values for compactional porosity loss have relatively remained similar both at and away from the sill contact (Figure 15E). This is presumably because the sill intrusions are relatively thin (0.4–4 m) and, thus, could not exert enough vertical loading on the sandstones to cause significant compaction. However,

cementational porosity loss decreases outwards from the sill contact, probably because the acidic fluids supplied by the intrusions have caused the dissolution of early calcite, creating secondary intergranular porosity (Figure 14E). In addition, the increase in cementational porosity loss away from the contact has been contributed by the increasing kaolinite and dickite from muscovite, due to its density and hydrodynamic processes. Overall, porosity is reduced mainly due to compaction rather than cementation.

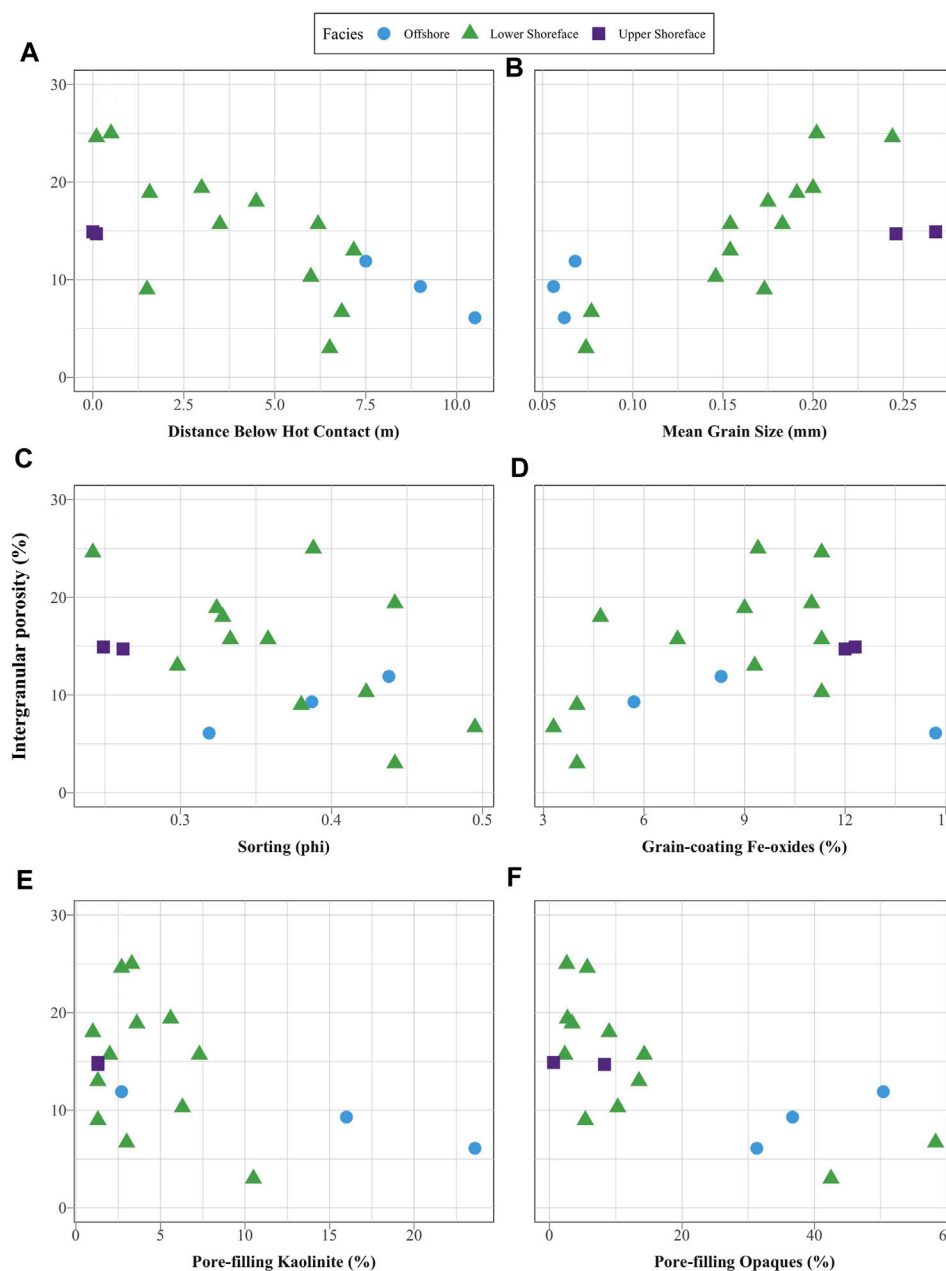


FIGURE 18 Controls on intergranular porosity. (A) An increase in porosity towards the sill contact. (B) An increase in porosity with increasing mean grain size. (C) An increase in porosity with better sorting. (D) An increase in porosity with increasing amount of grain-coating Fe-oxide minerals. (E) A decrease in porosity with increasing kaolinite content. (F) A decrease in porosity with increasing pore-filling Fe-oxide content.

6 Conclusion

- The studied Qasim Formation consists of coarse silt to medium grained sandstones, deposited in offshore, lower and upper shoreface depositional settings. The sandstones are primarily quartz arenites in composition.
- The best intergranular porosity in the Qasim Formation (up to 25%) was recorded in the sandstones with coarser grain size, better sorting, and lower percentage of pore-filling kaolinite, dickite, calcite, and iron oxide cements.
- Porosity evolution in the sandstones is strongly influenced by eodiagenesis, telodiagenesis, and sill-induced diagenesis. Mechanical compaction is the most important shallow-burial, eogenetic process through which porosity is reduced compared to cementation. Kaolinite is the most abundant eogenetic cement, formed mainly from alteration of muscovite.
- Telogenetic alterations, related to uplift, include the partial to pervasive dissolution of early calcite, oxidation of pyrite to hematite, and formation of goethite, presumably due to circulation of Fe-rich, oxidizing groundwater.

- The main sill-induced diagenetic alterations in the Qasim Formation, related to the Tertiary basaltic intrusions, include the dissolution of detrital quartz grains and rounded quartz overgrowths, transformation of kaolinite into dickite and, to some extent, formation of angular quartz overgrowths and conversion of kaolinite into chlorite.
- Because the Qasim Formation (Quwarah Member) experienced only shallow burial prior to the basaltic-sill intrusions, the magma is believed to have provided the requisite acidic conditions and temperature for the dissolution of quartz grains and the conversion of kaolinite into dickite and chlorite. The required Fe for the formation of chlorite was likely to have been supplied from the dissolution of goethite.
- The formation of dickite from kaolinite was found to be facies dependent, with the dickite being more abundant in the offshore depositional setting than in the lower and upper shoreface, chiefly because of the increase in abundance of muscovite in the offshore environment than in the other two depositional settings.
- The extent of magmatic-induced alterations in sandstones largely depends on their composition, the type and temperature of the magma, and the duration to which the sandstones were exposed to heat from the magma.

Data availability statement

The original contributions presented in the study are included in the article/supplementary material further inquiries can be directed to the corresponding authors.

Author contributions

AB: Conceptualization; Data curation; Formal analysis; Investigation; Methodology; Software; Validation; Visualization; Writing—original draft; Writing—review and editing. KA-R: Funding acquisition; Project administration; Resources; Software; Supervision; Validation; Visualization; Writing—review and editing. AK: Resources; Validation; Visualization; Writing—review and editing. AA: Resources; Software; Validation; Visualization;

References

- Aarnes, I., Svensen, H., Polteau, S., and Planke, S. (2011). Contact metamorphic devolatilization of shales in the Karoo Basin, South Africa, and the effects of multiple sill intrusions. *Chem. Geol.* 281, 181–194. doi:10.1016/j.chemgeo.2010.12.007
- Al-Ramadan, K. A., Hussain, M., Imam, B., and Saner, S. (2004). Lithologic characteristics and diagenesis of the devonian jauf sandstone at ghawar field, eastern Saudi Arabia. *Mar. Petroleum Geol.* 21, 1221–1234. doi:10.1016/j.marpetgeo.2004.09.002
- Al-Ramadan, K., Franks, S. G., Al-Shammari, S., Rees, A., Koeshidayatullah, A., and Abu-Khamsin, S. (2017). Depositional and diagenetic barriers, baffles and conduits: Permian – carboniferous unayzah reservoir, nuayyim field, central Saudi Arabia. *J. Petroleum Geol.* 40, 85–103. doi:10.1111/jpg.12665
- Al-Ramadan, K., Koeshidayatullah, A., Cantrell, D., and Swart, P. K. (2019). Impact of basin architecture on diagenesis and dolomitization in a fault-bounded carbonate platform: Outcrop analogue of a pre-salt carbonate reservoir, Red Sea rift, NW Saudi Arabia. *PG* 26, 448–461. doi:10.1144/petgeo2018-125
- Al-Ramadan, K., Morad, S., Norton, A. K., and Hulver, M. (2013). “Linking diagenesis and porosity preservation versus destruction to sequence stratigraphy of gas condensate reservoir sandstones; the Jauf Formation (Lower to Middle Devonian), Eastern Saudi Arabia,” in *Linking diagenesis to sequence Stratigraphy* (Chichester, West Sussex, UK: Wiley-Blackwell), 297–336.
- Al-Ramadan, K., Morad, S., Proust, J. N., and Al-Aasm, I. (2005). Distribution of diagenetic alterations in siliciclastic shoreface deposits within a sequence stratigraphic framework: Evidence from the Upper Jurassic, Boulonnais, NW France. *J. Sediment. Res.* 75, 943–959. doi:10.2110/jsr.2005.072
- Al-Ramadan, K. (2021). The role of diagenesis at unconformities of the paleozoic siliciclastic succession of central Saudi Arabia: Implications for reservoir quality. *Arabian J. Geosciences* 14, 484. doi:10.1007/s12517-021-06845-6
- Allen, M. J., Faulkner, D. R., Worden, R. H., Rice-Birchall, E., Katirtsidis, N., and Utley, J. E. P. (2020). Geomechanical and petrographic assessment of a CO₂ storage site: Application to the Acorn CO₂ Storage Site, offshore United Kingdom. *Int. J. Greenh. Gas Control* 94, 102923. doi:10.1016/j.jggc.2019.102923

Writing—review and editing. AH: Formal analysis; Validation; Visualization; Writing—review and editing. FA-G: Formal analysis; Validation; Visualization; Writing—review and editing. MM: Formal analysis; Validation; Visualization; Writing—review and editing.

Funding

This study is supported by the King Fahd University of Petroleum and Minerals, Saudi Arabia (Grant Number: SF 19003).

Acknowledgments

We are grateful to Mr. Habeeb A. Al-Abbas and Mr Bandar O. Al-Otaibi for preparation of thin sections and XRD analysis, respectively. Special thanks go to Mr Idrees Farooqui for reproduction of geological maps of the studied quadrangle. The authors are immensely grateful to Abdullah Alqubalee for running QEMSCAN analysis. The authors would like to thank the Associate Editor Ángel Puga-Bernabéu, Ahmed E. Radwan and one reviewer for their constructive comments and reviews, which greatly assisted in improving the quality of the manuscript.

Conflict of interest

The authors declare that the research was conducted in the absence of any commercial or financial relationships that could be construed as a potential conflict of interest.

Publisher's note

All claims expressed in this article are solely those of the authors and do not necessarily represent those of their affiliated organizations, or those of the publisher, the editors and the reviewers. Any product that may be evaluated in this article, or claim that may be made by its manufacturer, is not guaranteed or endorsed by the publisher.

- Amao, A. O., Al-Otaibi, B., and Al-Ramadan, K. (2022). High-resolution X-ray diffraction datasets: Carbonates. *Data Brief* 42, 108204. doi:10.1016/j.dib.2022.108204
- Amao, A. O., Al-Ramadan, K., and Koeshidayatullah, A. (2016). Automated mineralogical methodology to study carbonate grain microstructure: An example from oncoids. *Environ. Earth Sci.* 75, 666. doi:10.1007/s12665-016-5492-x
- Aro, O. E., Jones, S. J., Meadows, N. S., Gluyas, J., and Charlaftis, D. (2023). *The importance of facies, grain size, and clay content in controlling fluvial reservoir quality – an example from the Triassic Skagerrak Formation*. Central North Sea, UK: PG. doi:10.1144/petgeo2022-043
- Bahlis, A. B., and de Ros, L. F. (2013). Origin and impact of authigenic chlorite in the Upper Cretaceous sandstone reservoirs of the Santos Basin, eastern Brazil. *Pet. Geosci.* 19, 185–199. doi:10.1144/petgeo2011-007
- Beaufort, D., Cassagnabere, A., Petit, S., Lanson, B., Berger, G., Lachapagne, J. C., et al. (1998). Kaolinite-to-dickite reaction in sandstone reservoirs. *Clay Min.* 33, 297–316. doi:10.1180/000985598545499
- Bello, A. M., Al-Ramadan, K., Babalola, L. O., Alqubalee, A., and Amao, A. O. (2023a). Impact of grain-coating illite in preventing quartz cementation: Example from permocarboniferous sandstone, Central Saudi Arabia. *Mar. Petroleum Geol.* 149, 106073. doi:10.1016/j.marpetgeo.2022.106073
- Bello, A. M., Butt, M. N., Hussain, A., Amao, A. O., Olariu, C., Koeshidayatullah, A. I., et al. (2023b). Impact of depositional and diagenetic controls on reservoir quality of syn-rift sedimentary systems: An example from oligocene-miocene Al wajh formation, northwest Saudi Arabia. *Sediment. Geol.* 446, 106342. doi:10.1016/j.sedgeo.2023.106342
- Bello, A. M., Charlaftis, D., Jones, S. J., Gluyas, J., Acikalin, S., Cartigny, M., et al. (2022b). Experimental diagenesis using present-day submarine turbidite sands. *Front. Earth Sci.* 10, 952690. doi:10.3389/feart.2022.952690
- Bello, A. M., Jones, S. J., Gluyas, J., Acikalin, S., and Cartigny, M. (2021). Role played by clay content in controlling reservoir quality of submarine fan system, Forties Sandstone Member, Central Graben, North Sea. *Mar. Petroleum Geol.* 128, 105058. doi:10.1016/j.marpetgeo.2021.105058
- Bello, A. M., Jones, S. J., Gluyas, J., and Al-Ramadan, K. (2022a). Impact of grain-coating clays on porosity preservation in paleocene turbidite channel sandstones: Nelson oil field, UK central North sea. *Minerals* 12, 555. doi:10.3390/min12050555
- Bello, A. M., Usman, M. B., Usman, A., Al-Ramadan, K., Babalola, L. O., Amao, A. O., et al. (2022c). Role of diagenetic alterations on porosity evolution in the cretaceous (Albian-Aptian) Bima Sandstone, a case study from the Northern Benue Trough, NE Nigeria. *Mar. Petroleum Geol.* 145, 105851. doi:10.1016/j.marpetgeo.2022.105851
- Berner, R. A. (1969). Goethite stability and the origin of red beds. *Geochimica Cosmochimica Acta* 33, 267–273. doi:10.1016/0016-7037(69)90143-4
- Bjørlykke, K., Aagaard, P., Egeberg, P. K., and Simmons, S. P. (1995). “Geochemical constraints from formation water analyses from the North Sea and the Gulf Coast Basins on quartz, feldspar and illite precipitation in reservoir rocks,” in *Geological society special publication*. Editor W. A. Cubitt (England: Spec. Publ. Geol. Soc. London), 33–50. doi:10.1144/GSL.SP.1995.086.01.03
- Bjørlykke, K. (1988). “Chapter 2 sandstone diagenesis in relation to preservation, destruction and creation of porosity,” in *Developments in sedimentology* (California: Elsevier Publishing Company), 555–588. doi:10.1016/S0070-4571(08)70180-8
- Blake, R. E., and Walter, L. M. (1999). Kinetics of feldspar and quartz dissolution at 70–80°C and near-neutral pH: Effects of organic acids and NaCl. *Geochimica Cosmochimica Acta* 63, 2043–2059. doi:10.1016/S0016-7037(99)00072-1
- Bloch, S. (1994). Effect of DeTrital mineral composition on reservoir quality. *SEPM Soc. Sediment. Geol.* 30, 161. doi:10.2110/10/scn.94.30.0161
- Bloch, S., Lander, R. H., and Bonnell, L. (2002). Anomalously high porosity and permeability in deeply buried sandstone reservoirs: Origin and predictability. *AAPG Bull.* 86, 301–328. doi:10.1306/61eedabc-173e-11d7-8645000102c1865d
- Boles, J. R., and Franks, S. G. (1979). Clay diagenesis in Wilcox sandstones of Southwest Texas; implications of smectite diagenesis on sandstone cementation. *J. Sediment. Res.* 49, 55–70. doi:10.1306/212F76BC-2B24-11D7-8648000102C1865D
- Busigny, V., and Dauphas, N. (2007). Tracing paleofluid circulations using iron isotopes: A study of hematite and goethite concretions from the Navajo sandstone (Utah, USA). *Earth Planet. Sci. Lett.* 254, 272–287. doi:10.1016/j.epsl.2006.11.038
- Chan, M. A., Parry, W. T., and Bowman, J. R. (2000). Diagenetic hematite and manganese oxides and fault-related fluid flow in jurassic sandstones, southeastern Utah. *Bulletin* 84, 1865. doi:10.1306/A9673E82-1738-11D7-8645000102C1865D
- Chen, G., Du, G., Zhang, G., Wang, Q., Lv, C., and Chen, J. (2011). Chlorite cement and its effect on the reservoir quality of sandstones from the Panyu low-uptift, Pearl River Mouth Basin. *Petroleum Sci.* 8, 143–150. doi:10.1007/s12182-011-0127-z
- Chen, G., Liu, H., Tang, Y., Niu, Z., Yu, J., and Bian, B. (2021). Effects of diabase intrusions on surrounding clastic rock reservoir in early diagenetic stages: A case study of the early permian fengcheng Formation in the dabasong uplift, junggar basin. *Interpretation* 9, T1157–T1165. doi:10.1190/INT-2021-0004.1
- Chen, X., Qu, X. Y., Qiu, L. W., Song, T. S., and Zhang, L. Q. (2015). Hydrothermal experiment research on characteristics and mechanisms of quartz dissolution. *Bull. Mineralogy Petrology Geochem.* 34, 1027–1033. doi:10.3969/j.issn.1007-2802.2015.05.019
- Chuhan, F. A., Kjeldstad, A., Bjørlykke, K., and Høeg, K. (2002). Porosity loss in sand by grain crushing—Experimental evidence and relevance to reservoir quality. *Mar. Petroleum Geol.* 19, 39–53. doi:10.1016/S0264-8172(01)00049-6
- Craigie, N. W., and Rees, A. J. (2016). Chemostratigraphy of glaciomarine sediments in the sarah formation, northwest Saudi Arabia. *J. Afr. Earth Sci.* 117, 263–284. doi:10.1016/j.jafrearsci.2016.02.006
- Dott, R. H., and Bourgeois, J. (1982). Hummocky stratification: Significance of its variable bedding sequences. *GSA Bull.* 93, 663–680. doi:10.1130/0016-7606(1982)93<663:HSSOIV>2.0.CO;2
- Duffy, M., Farrell, N., Raeside, R., Muirhead, D., Healy, D., Brasier, A., et al. (2021). Observations of reservoir quality alteration in proximity to igneous intrusions for two distinct sandstones in Scotland. *Mar. Petroleum Geol.* 129, 105071. doi:10.1016/j.marpetgeo.2021.105071
- Ehrenberg, S. N., Aagaard, P., Wilson, M. J., Fraser, A. R., and Duthie, D. M. L. (1993). Depth-dependent transformation of kaolinite to dickite in sandstones of the Norwegian continental shelf. *Clay Miner.* 28, 325–352. doi:10.1180/claymin.1993.028.3.01
- Ehrenberg, S. N. (1993). Preservation of anomalously high porosity in deeply buried sandstones by grain-coating chlorite: Examples from the Norwegian continental shelf. *AAPG Bull.* 77, 1260–1286.
- Eide, C. H., Schofield, N., Jerram, D. A., and Howell, J. A. (2017). Basin-scale architecture of deeply emplaced sill complexes: Jameson Land, East Greenland. *J. Geol. Soc.* 174, 23–40. doi:10.1144/jgs2016-018
- Einsele, G., Gieskes, J. M., Curray, J., Moore, D. M., Aguayo, E., Aubry, M. P., et al. (1980). Intrusion of basaltic sills into highly porous sediments, and resulting hydrothermal activity. *Nature* 283, 441–445. doi:10.1038/283441a0
- Feng, Q., and Tang, X. Y. (1997). Magma activity's influence on conditions forming oil and gas pools. *Geol. Sci. Technol. Inf.* 16, 59–65.
- Folk, R. L. (1980). *Petrology of sedimentary rocks*. Austin, Texas: Hemphill Publishing Company.
- Grainger, D. J., and Hanif, M. R. (1989). “Explanatory notes to the geological map of the Shaghab quadrangle, Sheet 27B, kingdom of Saudi Arabia,” in *Ministry of Petroleum and mineral Resources* (Riyadh, Saudi Arabia: Ministry of Petroleum and Mineral Resources), 2–30.
- Grove, C., Jerram, D. A., Gluyas, J. G., and Brown, R. J. (2017). Sandstone diagenesis in sediment-lava sequences: Exceptional examples of volcanically driven diagenetic compartmentalization in dune valley, huab outliers, nw Namibia. *J. Sediment. Res.* 87, 1314–1335. doi:10.2110/jsr.2017.75
- Haile, B. G., Czarniecka, U., Xi, K., Smyrak-Sikora, A., Jahren, J., Braathen, A., et al. (2019). Hydrothermally induced diagenesis: Evidence from shallow marine-deltaic sediments, Wilhelmøya, Svalbard. *Geosci. Front.* 10, 629–649. doi:10.1016/j.gsf.2018.02.015
- Hakimi, M. H., Shalaby, M. R., and Abdullah, W. H. (2012). Diagenetic characteristics and reservoir quality of the lower cretaceous biyadh sandstones at kharir oilfield in the Western central masila basin, Yemen. *J. Asian Earth Sci.* 51, 109–120. doi:10.1016/j.jseaes.2012.03.004
- Heald, M. T. (1955). Stylolites in sandstones. *J. Geol.* 63, 101–114. doi:10.1086/626237
- Hellevang, H., Line, L. H., Eide, C. H., Jahren, J., and Haile, B. G. (2021). Insights into past tectonism from authigenic quartz. *Geochem. Persp. Lett.* 19, 27–31. doi:10.7185/geochemlet.2130
- Herlambang, A., Koeshidayatullah, A. I., Amao, A. O., Bello, A. M., Al-Ghamdi, F., Malik, M. H., et al. (2022). Structural diagenesis and dolomitization of cenozoic post-rift carbonates in the red sea rift basin: A multiproxy approach. *Front. Earth Sci.* 10, 1–15. doi:10.3389/feart.2022.1037126
- Holford, S., Schofield, N., Jackson, C. L., Magee, C., Green, P., and Duddy, I. (2013). “Impacts of igneous intrusions on source reservoir potential in prospective sedimentary basins along the western Australian continental margin,” in *West Australian basins symposium* (Clayton South, Australia: The Australian Petroleum Production & Exploration Association (APPEA)).
- Holford, S., Schofield, N., MacDonald, J., Duddy, I., and Green, P. (2012). Seismic analysis of igneous systems in sedimentary basins and their impacts on hydrocarbon prospectivity: Examples from the southern Australian margin. *APPEA J.* 52, 229. doi:10.1071/AJ11017
- Hussain, A., Butt, M. N., Olariu, C., Malik, M. H., Koeshidayatullah, A., Amao, A., et al. (2022). Unravelling reservoir quality heterogeneity in mixed siliciclastic-carbonate deposits: An example from Miocene Red Sea rift, NW Saudi Arabia. *Mar. Petroleum Geol.* 145, 105850. doi:10.1016/j.marpetgeo.2022.105850
- Hussain, A., Morris, E. A., Al-Ramadan, K., Shannon, P. M., and Houghton, P. D. W. (2023). Hybrid event beds (HEBs) and the ‘greywacke problem’ revisited. *Earth-Science Rev.* 237, 104297. doi:10.1016/j.earscirev.2022.104297
- Hussain, M., and Abdullatif, O. M. (2004). *Trace element Geochemistry and heavy mineral assemblage of the cambro-ordovician Saq sandstone of the Tabuk basin and its possible correlation with the wajid sandstone of the wajid basin, southwest Saudi Arabia*. Saudi Arabia: KACST Project.
- Hussain, M., Amao, A., Jin, G., and Al-Ramadan, K. (2018). “Linking geochemical and mechanical properties of rock samples using new non-destructive techniques,” in *SPE kingdom of Saudi Arabia annual technical symposium and exhibition* (Dammam, Saudi Arabia: SPE). doi:10.2118/192347-MS

- Karlsen, A. D., Dahlgren, S., Jarntveit, B., and Kjærnet, T. (1998). "Thermal effects of basaltic sill emplacement in source rocks for maturation and hydrocarbon generation," in *60th EAGE conference and exhibition* (Leipzig, Germany: European Association of Geoscientists & Engineers). doi:10.3997/2214-4609.201408501
- Ketzer, J. M., Morad, S., and Amorosi, A. (2003). "Predictive diagenetic clay-mineral distribution in siliciclastic rocks within a sequence stratigraphic framework," in *Clay mineral cements in sandstones*. Editors R. H. Worden and S. Morad (Oxford, UK: Blackwell Publishing Ltd.), 43–61. doi:10.1002/9781444304336.ch2
- Knauss, K. G., and Wolery, T. J. (1988). The dissolution kinetics of quartz as a function of pH and time at 70°C. *Geochimica Cosmochimica Acta* 52, 43–53. doi:10.1016/0016-7037(88)90055-5
- Koeshidayatullah, A., and Al-Ramadan, K. (2014). Unraveling cementation environment and patterns of holocene beachrocks in the arabian gulf and the gulf of aqaba: Stable isotope approach. *GQ* 58, 1144. doi:10.7306/gq.1144
- Laboun, A. A. (2010). Paleozoic tectono-stratigraphic framework of the arabian peninsula. *J. King Saud Univ. - Sci.* 22, 41–50. doi:10.1016/j.jksus.2009.12.007
- Lanson, B., Beaufort, D., Berger, G., Baradat, J., and Lachapagne, J. C. (1996). Illitization of diagenetic kaolinite-to-dickite conversion series; late-stage diagenesis of the Lower Permian Rotliegend Sandstone reservoir, offshore of The Netherlands. *J. Sediment. Res.* 66, 501–518. doi:10.1306/D4268392-2B26-11D7-8648000102C1865D
- Lanson, B., Beaufort, D., Berger, G., Bauer, A., Cassagnabère, A., and Meunier, A. (2002). Authigenic kaolin and illitic minerals during burial diagenesis of sandstones: A review. *Clay Miner.* 37, 1–22. doi:10.1180/0009855023710014
- Lundegard, P. D. (1992). Sandstone porosity loss - a "big picture" view of the importance of compaction. *J. Sediment. Petrology* 62, 250–260. doi:10.1306/d426784d-2b26-11d7-8648000102c1865d
- Manivit, J., Vaslet, D., Berthiaux, A., Le Strat, P., and Fourniguet, J. (1986). *Geologic map of the Buraydah quadrangle, sheet 26G, kingdom of Saudi Arabia*. Saudi Arabia: U.S. Geological Survey.
- Mansurbeg, H., Morad, S., Salem, A., Marfil, R., El-ghali, M. A. K., Nystuen, J. P., et al. (2008). Diagenesis and reservoir quality evolution of palaeocene deep-water, marine sandstones, the Shetland-Faroes Basin, British continental shelf. *Mar. Petroleum Geol.* 25, 514–543. doi:10.1016/j.marpetgeo.2007.07.012
- Marchand, A. M. E., Apps, G., Li, W., and Rotzien, J. R. (2015). Depositional processes and impact on reservoir quality in deepwater Paleogene reservoirs, US Gulf of Mexico. *AAPG Bull.* 99, 1635–1648. doi:10.1306/04091514189
- Marfil, R., Delgado, A., Rossi, C., Iglesia, A. L., and Ramseyer, K. (2003). Origin and diagenetic evolution of kaolin in reservoir sandstones and associated shales of the jurassic and cretaceous, salam field, western desert (Egypt). *Clay Mineral Cem. Sandst.* 34, 317–342. doi:10.1002/9781444304336.ch14
- McGillivray, J. G., and Hussein, M. I. (1992). The paleozoic petroleum geology of central Arabia 1. *AAPG Bull.* 76, 1473–1490. doi:10.1306/BDF8A1A-1718-11D7-8645000102C1865D
- Mckinley, J. M., Worden, R. H., and Ruffell, A. H. (2001). Contact diagenesis: The effect of an intrusion on reservoir quality in the triassic sherwood sandstone group, northern Ireland. *J. Sediment. Res.* 71, 484–495. doi:10.1306/2DC40957-0E47-11D7-8643000102C1865D
- Monreal, R. F., Villar, H. J., Baudino, R., Delpino, D., and Zencich, S. (2009). Modeling an atypical petroleum system: A case study of hydrocarbon generation, migration and accumulation related to igneous intrusions in the neougen basin, Argentina. *Mar. Petroleum Geol.* 26, 590–605. doi:10.1016/j.marpetgeo.2009.01.005
- Morad, S., Al-Ramadan, K., Ketzer, J. M., and De Ros, L. F. (2010). The impact of diagenesis on the heterogeneity of sandstone reservoirs: A review of the role of depositional facies and sequence stratigraphy. *AAPG Bull.* 94, 1267–1309. doi:10.1306/04211009178
- Morad, S., Ismail, H. N. B., De Ros, L. F., Al-Aasm, I. S., and Serrhini, N. -E. (1994). Diagenesis and formation water chemistry of Triassic reservoir sandstones from southern Tunisia. *Sedimentology* 41, 1253–1272. doi:10.1111/j.1365-3091.1994.tb01452.x
- Morad, S., Ketzer, J. M., and De Ros, L. R. (2000). Spatial and temporal distribution of diagenetic alterations in siliciclastic rocks: Implications for mass transfer in sedimentary basins. *Sedimentology* 47, 95–120. doi:10.1046/j.1365-3091.2000.00007.x
- Moraes, M. A. S., and De Ros, L. F. (1992). "Depositional, infiltrated and authigenic clays in fluvial sandstones of the jurassic sergi formation, recôncavo basin, northeastern Brazil," in *Origin, diagenesis, and petrophysics of clay minerals in sandstones* (Brazil: Society of Economic Paleontologists and Mineralogists Special Publication), 197–208. doi:10.2110/pec.92.47.0197
- Muirhead, D. K., Bowden, S. A., Parnell, J., and Schofield, N. (2017). Source rock maturation owing to igneous intrusion in rifted margin petroleum systems. *J. Geol. Soc.* 174, 979–987. doi:10.1144/jgs2017-011
- Ochoa, M., Arribas, J., Mas, R., and Goldstein, R. H. (2007). Destruction of a fluvial reservoir by hydrothermal activity (Camereros Basin, Spain). *Sediment. Geol.* 202, 158–173. doi:10.1016/j.sedgeo.2007.05.017
- Oluwadebi, A. G., Taylor, K. G., and Dowe, P. J. (2018). Diagenetic controls on the reservoir quality of the tight gas collyhurst sandstone formation, lower permian, east Irish sea basin, United Kingdom. *Sediment. Geol.* 371, 55–74. doi:10.1016/j.sedgeo.2018.04.006
- Powers, R. W., Ramirez, L. F., Redmond, C. D., and Elberg, E. L. (1966). *Geology of the arabian peninsula - sedimentary geology of Saudi Arabia*. Saudi Arabia: US Geological Survey Professional. doi:10.3133/pp560D
- Rong, H., Jiao, Y., Wu, L., Zhao, X., Cao, M., and Liu, W. (2021). Effects of igneous intrusions on diagenesis and reservoir quality of sandstone in the Songliao Basin, China. *Mar. Petroleum Geol.* 127, 104980. doi:10.1016/j.marpetgeo.2021.104980
- Sanderson, I. D. (1984). Recognition and significance of inherited quartz overgrowths in quartz arenites. *J. Sediment. Res.* 54, 473–486. doi:10.1306/212F844A-2B24-11D7-8648000102C1865D
- Saner, S., Hassan, H. M., Al-Ramadan, K. A., and Abdulghani, W. M. (2006). Mineralogical, pore and petrophysical characteristics of the devonian jauf sandstone reservoir, hawiyah field, eastern Saudi Arabia. *J. Pet. Geol.* 29, 257–272. doi:10.1111/j.1747-5457.2006.00257.x
- Schofield, N., Holford, S., Millett, J., Brown, D., Jolley, D., Passey, S. R., et al. (2017). Regional magma plumbing and emplacement mechanisms of the faroe-shetland sill complex: Implications for magma transport and petroleum systems within sedimentary basins. *Basin Res.* 29, 41–63. doi:10.1111/bre.12164
- Senalp, M., and Al-Duaiji, A. A. (2001). Qasim Formation: Ordovician storm- and tide-dominated shallow-marine siliciclastic sequences, central Saudi Arabia. *GeoArabia* 6, 233–268. doi:10.2113/geoarabia0602233
- Senger, K., Millett, J., Planke, S., Ogata, K., Haug Eide, C., Festøy, M., et al. (2017). Effects of igneous intrusions on the petroleum system: A review. *First Break* 35, 11. doi:10.3997/1365-2397.2017011
- Senger, K., Tveranger, J., Ogata, K., Braathen, A., and Planke, S. (2014). Late mesozoic magmatism in svalbard: A review. *Earth-Science Rev.* 139, 123–144. doi:10.1016/j.earscirev.2014.09.002
- SGS (2013). Phanerozoic stratigraphy of Saudi Arabia Part 1 – paleozoic successions of the arabian shelf (cover rocks). *J. King Saud Univ. - Sci.* 22, 41–50.
- Sharland, P. R., Archer, D. M., Casey, R. B., Davies, S. H., Hall, A. P., Heward, A. D., et al. (2001). *Arabian Plate sequence Stratigraphy*. Manama, Bahrain: Gulf Petrolink, 371.
- Sleveland, A. R. N., Midtkandal, I., Galland, O., and Leanza, H. A. (2020). Sedimentary architecture of storm-influenced tidal flat deposits of the upper mulichinco formation, neuquén basin, Argentina. *Front. Earth Sci.* 8, 219. doi:10.3389/feart.2020.00219
- Steineke, M., Bramkamp, R. A., and Sander, N. J. (1958). *Stratigraphic relations of arabian jurassic oil*. New York: American Association of Petroleum Geologist (AAPG). doi:10.1306/SV18350C52
- Strother, P. K., Traverse, A., and Vecoli, M. (2015). Cryptospores from the Hanadir shale member of the Qasim Formation, ordovician (darrivillan) of Saudi Arabia: Taxonomy and systematics. *Rev. Palaeobot. Palynology* 212, 97–110. doi:10.1016/j.revpalbo.2014.08.018
- Swift, D. J. P., Figueiredo, A. G., Freeland, G. L., and Oertel, G. F. (1983). Hummocky cross-stratification and megaripples: a geological double standard? *J. Sediment. Res.* 53, 1295–1317. doi:10.1306/212F8369-2B24-11D7-8648000102C1865D
- Sydnos, M., Fjeldskaar, W., Grunnaleite, I., Fjeldskaar Lotveit, I., and Mjelde, R. (2019a). Transient thermal effects in sedimentary basins with normal faults and magmatic sill intrusions—a sensitivity study. *Geosciences* 9, 160. doi:10.3390/geosciences9040160
- Sydnos, M., Fjeldskaar, W., Grunnaleite, I., Lotveit, I. F., and Mjelde, R. (2019b). The influence of magmatic intrusions on diagenetic processes and stress accumulation. *Geosciences* 9, 477. doi:10.3390/geosciences9110477
- Vaslet, D., Kellogg, K. S., Berthiaux, A., Le Strat, P., and Vincent, P. L. (1987). *Geologic map of the Baq'a quadrangle, sheet 27F, kingdom of Saudi Arabia*. Saudi Arabia: Deputy Ministry for Mineral Resources.
- Vaslet, D. (1990). Upper ordovician glacial deposits in Saudi Arabia. *Episodes* 13, 147–161. doi:10.18814/epiugs/1990/v13i3/002
- Walker, R. G., Duke, W. L., and Leckie, D. A. (1983). Hummocky stratification: Significance of its variable bedding sequences: Discussion and reply. *GSA Bull.* 94, 1245–1249. doi:10.1130/0016-7606(1983)94<1245:hssov>2.0.co;2
- Worden, R. H., Armitage, P. J., Butcher, A. R., Churchill, J. M., Csoma, A. E., Hollis, C., et al. (2018). "Petroleum reservoir quality prediction: Overview and contrasting approaches from sandstone and carbonate communities," in *Geological society special publication*. Editors J. O. P. J. Armitage, A. Butcher, J. Churchill, A. Csoma, C. Hollis, R. H. Lander, et al. (London: Geological Society, London, Special Publications), 1–31. doi:10.1144/SP435.21
- Worden, R. H., Griffiths, J., Wooldridge, L. J., Utey, J. E. P., Lawan, A. Y., Muhammed, D. D., et al. (2020). Chlorite in sandstones. *Earth-Science Rev.* 204, 103105. doi:10.1016/j.earscirev.2020.103105
- Worden, R. H., and Morad, S. (2003). "Clay minerals in sandstones: Controls on formation, distribution and evolution," in *Clay mineral cements in sandstones* (Oxford, UK: Blackwell Publishing Ltd.), 1–41. doi:10.1002/9781444304336.ch1
- Xia, C., and Wilkinson, M. (2017). The geological risks of exploring for a CO2 storage reservoir. *Int. J. Greenh. Gas Control* 63, 272–280. doi:10.1016/j.jggc.2017.05.016
- Zahedi, M. K., and MacDonald, S. (2018). Volcanics: A commonly underestimated part of petroleum exploration. *ASEG Ext. Abstr.* 2018 1–6. doi:10.1071/ASEG2018abP061
- Zhang, S., and Liu, Y. (2014). Molecular-level mechanisms of quartz dissolution under neutral and alkaline conditions in the presence of electrolytes. *Geochem. J.* 48, 189–205. doi:10.2343/geochemj.2.0298